

ABSTRACT

Title of Thesis: UTILIZING A HIGH-RESOLUTION CFD-BASED MODEL TO REPLICATE THE BURNING OF A TWO-STORY STRUCTURE IN THE MAUI WILDFIRE

Evan Thomas Gironda, Master of Science, 2025

Thesis Directed By: Dr. Shuna Ni, Department of Fire Protection Engineering

The Wildland-Urban Interface (WUI), the area where structures and other human development meet with undeveloped wildland, grows by millions of acres per year in the United States. The WUI experiences unique challenges when considered in the realm of fire protection engineering, with potential fires in the WUI endangering tens of thousands of communities nationwide. On August 8, 2023, one such fire devastated the historic Lahaina town in Maui, Hawaii, destroying over a thousand structures. This project uses the NIST Fire Dynamics Simulator (FDS) to recreate a part of the fire that destroyed two neighboring residences in Lahaina. Detailed models and configurations are created to replicate wind, vegetative fuel combustion, and structural burning. Results of the simulation show that the use of a half-wall height burner configuration in an optically thin radiation model best recreated the flame spread between adjacent structures and vegetative fuels. Models qualitatively demonstrate flame spread between structures; however, quantitative timing is highly sensitive to uncertainty. Sensitivity analysis suggests that the emissivity of a structure's outermost layer is the primary source of uncertainty in model results.

UTILIZING A HIGH-RESOLUTION CFD-BASED MODEL TO REPLICATE THE
BURNING OF A TWO-STORY STRUCTURE IN THE MAUI WILDFIRE

by

Evan Thomas Girona

Thesis submitted to the Faculty of the Graduate School of the
University of Maryland, College Park, in partial fulfillment
of the requirements for the degree of
Master of Science
2025

Advisory Committee:
Dr. Shuna Ni, Chair
Dr. Arnaud Trouve
Dr. Stanislav Stoliarov

© Copyright by
Evan Thomas Gironda
2025

Acknowledgements

I am extremely grateful for all the support I have received during this project. First and foremost, I would like to thank my committee chair and primary supervisor, Dr Shuna Ni. Her guidance and support throughout this project were much needed and helped with many of the technical and mental challenges that arose over the past year. I would also like to thank Dr Arnaud Trouve and Dr Stanislav Stoliarov, who along with Dr Ni gave the guidance during all of our meetings, which continuously supplied me not just with the direction but also the confidence I needed to complete this research. I would be remiss if I did not acknowledge all the Department of Fire Protection Engineering's faculty, staff, and students. You have all created a warm and welcoming environment over the past 5 years that supports everyone through all types of hardship, and I cannot be prouder of my decision to study in this field.

I would like to thank all of my friends and family for helping me during the past year. Whether it was playing Dungeons & Dragons with me in the evenings, having a bit to eat together, or hanging out at football tailgates, your support was very much needed and appreciated in completing this project. Above all else, I want to thank my girlfriend, Jennifer. Without your support, I can guarantee I would not have been able to complete this project.

I want to give a special thanks to Dr Jonathan Hodges for his support with this project. His knowledge in FDS was critical for identifying how to best create and analyze my FDS models. I look forward greatly to working with you further at Jensen Hughes.

This project was made possible thanks to funding from the National Science Foundation (Award #2401876). The NSF's support for academic research is a boon to our society, as the research they fund inspires countless students worldwide to pursue STEM research.

The authors acknowledge the University of Maryland supercomputing resources (<http://hpcc.umd.edu>) made available for conducting the research reported in this paper.

Table of Content

Acknowledgements.....	ii
Table of Content	iv
List of Tables	vi
List of Figures.....	vii
Chapter 1 Introduction.....	1
1.1 Background	2
1.2 Motivation.....	3
1.3 Scope of Work.....	4
Chapter 2 Literature Review.....	6
2.1 Full Scale Testing.....	6
2.1.1 Structure Separation in WUI Environments	6
2.1.2 Flame Spread from Environmental Sources	8
2.2 Previous Modeling Efforts	8
2.2.1 Thermal Exposure in WUI Environments	9
2.2.2 Ember Accumulation and Transport.....	11
2.2.3 Structural Response	12
Chapter 3 Introduction of Lahaina Fire and Choice of Model Area	15
3.1 Lahaina Wildfire	15
3.1.1 Drivers of Rapid Fire Spread.....	15
3.1.2 Impact of the Wildfire to the Community.....	18
3.2 Selection of Model Area	20
3.2.1 Search for Viable Area.....	20
3.2.2 Details of Selected Model Area	21
Chapter 4 Model Development using FDS.....	24
4.1 Introduction of FDS	24
4.2 House Geometry and Construction	26
4.3 Burner Configurations.....	29
4.4 Design Fires for Level 1 and Level 2.....	31
4.5 Design Fires for Roof.....	35
4.6 Wind Configuration.....	37
4.7 Vegetative Fuels.....	39
4.8 Radiation Solver.....	43
4.9 Computational Domain	48
4.9.1 Domain Boundaries	48

4.9.2	Grid Resolution.....	50
4.9.3	Final Computational Domain.....	56
Chapter 5	Results and Discussion	59
5.1	Results from the Full-scale Models with Different Burner Configurations.....	59
5.2	Impact of Vegetation on Fire Spread between Structures.....	70
5.3	Impact of Wind Direction on Fire Spread Between Structures.....	72
5.4	Material Property Sensitivity Analysis	73
Chapter 6	Conclusion and Future Work.....	77
6.1	Summary of Work.....	77
6.2	Limitations and Future Work.....	78
Bibliography	81

List of Tables

Table 4.1 Exterior Wall Materials	27
Table 4.2 Material Properties.....	28
Table 4.3 Design Fire Parameters.....	32
Table 4.4 Design Fire Ignition Times.....	32
Table 4.5 Roof Heat Release Rates.....	36
Table 4.6 Vegetation Particles	42
Table 4.7 Mesh Sensitivity Model Mesh Count	53
Table 5.1 Sensitivity Analysis Properties	74
Table 5.2 Predicted Ignition Times.....	75

List of Figures

Figure 1.1 Selected Model Area	5
Figure 1.2 Security Camera Footage of 1267 and 1259 Nahale Pl.....	5
Figure 3.1 Lahaina Meteorological Conditions [30].....	17
Figure 3.2 Damaged and Undamaged Structures in Lahaina [36–39].....	19
Figure 3.3 Selected Model Area	22
Figure 3.4 Security Camera Footage	22
Figure 4.1 FDS Model Area.....	27
Figure 4.2 Roof Cross-Section [53].....	29
Figure 4.3 Wall Burner Locations (Burner surfaces are colored by red).....	30
Figure 4.4 1267 Nahale PI Ignition Point	32
Figure 4.5 Design Fire Ignition Time	33
Figure 4.6 Design Fire Profile [51].....	34
Figure 4.7 Heat Release Rates	34
Figure 4.8 Model End Time.....	35
Figure 4.9 Roof Fire Spread	37
Figure 4.10 Time-Velocity Function	38
Figure 4.11 Wind Direction	39
Figure 4.12 Vegetation Between Houses.....	40
Figure 4.13 Burning Vegetation	40
Figure 4.14 Douglas Fir FDS Validation [11]	42
Figure 4.15 Radiation Configuration Test Simulation.....	46
Figure 4.16 Radiation Parameter Tests (Optically thin selected)	46
Figure 4.17 Wind Development Model	49
Figure 4.18 Wind Velocity Development Test Results	50
Figure 4.19 Simplified Model for Mesh Sensitivity Studies	51
Figure 4.20 Example of Grid Alignment in the Simplified Model (with a minimum cell size of 5 cm)	52
Figure 4.21 Total Heat Flux at Target Wall.....	54
Figure 4.22 Radiative Heat Flux at Target Wall.....	54
Figure 4.23 Target Wall Surface Temperature	55
Figure 5.1 Heat Flux	60
Figure 5.2 Wall Surface Temperature.....	60
Figure 5.3 Corresponding Video Segment around the Estimated Ignition Time	62
Figure 5.4 Heat Flux Contours, 20cm Cell Resolution.....	63
Figure 5.5 Wall Temperature Contours, 20cm Cell Resolution	63
Figure 5.6 Tree Ignition (t=2070s).....	64
Figure 5.7 Tree Ignition, Half-Wall Burner.....	65
Figure 5.8 Video and FDS Model Comparison	67
Figure 5.9 Window Heat Flux	68
Figure 5.10 Interior Burner Configuration Heat Flux.....	70

Chapter 1 Introduction

In August 2023, a wildfire in western Maui decimated the town of Lahaina, claiming 102 lives, burning thousands of acres of land, and destroying or damaging 2,200 structures [1]. The devastation of the wildfire was driven by strong winds, a lack of active fire suppression, and Lahaina's downward-sloping coastal topography. However, some buildings throughout Lahaina survived the fire and seemed undamaged despite these exacerbating factors [2]. It is well within reason that the buildings survived not by mere coincidence, but rather due to features of their construction, including fire-resistant exterior siding, separation from adjacent structures, and landscaping on the property. Current models for wildfire spread in Wildland Urban Interface (WUI) settings operate well at larger scales, but fail at capturing observations from Lahaina that would explain buildings remaining undamaged amidst their destroyed neighbors. Computational Fluid Dynamics-based (CFD-based) software such as Fire Dynamics Simulator (FDS) in principle has the capability to create high-fidelity models of fire spread between individual structures. However, a lack of data necessary for accurate setup of the models has led to limited application. The goal of this project is to make use of NIST FDS to model the burning of an individual structure in Lahaina to establish an accurate heating input for the high-fidelity simulations of fire propagation to and through a neighboring structure. Discrepancies between observations in Lahaina and modeled fire behavior will be identified as they arise to establish where current understanding of models may be lacking or incomplete, to help guide further development of WUI modeling techniques.

1.1 Background

As human development continues to expand into previously undeveloped areas, the threat of wildfires in the Wildland-Urban Interface (WUI) has become increasingly significant. The U.S. Fire Administration defines the WUI as "the zone of transition between unoccupied land and human development [...] where structures and other human development meet or intermingle with undeveloped wildland or vegetative fuels." More than 60,000 communities across the United States are currently at risk of WUI fires, and between 2002 and 2016, an average of over 3,000 structures per year were lost to such events.

This growing risk is driven by the convergence of urban sprawl, population growth, and climate change. As cities expand and more people move into fire-prone regions, wildfires increasingly affect residential areas. At the same time, climate change has led to hotter, drier conditions, making vegetation more flammable and increasing the likelihood of ignition and rapid fire spread. Although the total number of wildfires and the global area burned decreased between 2005 and 2020, the proportion of fires occurring in WUI areas increased by 23%, and the area burned by WUI fires rose by 35% during the same period [5].

Several recent events have highlighted the severe consequences of WUI fires. In 2019, wildfires in Alberta, Canada, forced the evacuation of thousands of residents. In August 2023, a fire ignited on the island of Maui, Hawaii, which ultimately devastated the town of Lahaina, resulting in over 102 fatalities and the destruction of more than 2,200 structures [3,4]. In 2025, the Palisades and Eaton fires in Los Angeles, California, destroyed thousands of homes and further underscored the vulnerability of communities in WUI regions [6–8].

The increasing frequency and scale of these events point to the urgent need for improved fire modeling and risk assessment methods tailored to WUI settings. In particular, understanding

how fire spreads between residential structures and how specific building features contribute to survivability is critical for developing strategies to reduce fire impacts. While some buildings in WUI fires are completely destroyed, others in close proximity remain untouched. This suggests that construction characteristics, spacing, and other local factors may play a crucial role in fire resilience.[3][4–6]

1.2 Motivation

Full-scale fire experiments have been performed to help understand structure burning dynamics arising from WUI fires, however they typically are done with controlled conditions that may not fully represent all the conditions that may exist in a WUI setting. Structures in those tests are unable to represent all structures that may exist in a WUI setting. Unlike full-scale testing, high-fidelity Computational Fluid Dynamics (CFD) simulations can be used to model the diverse conditions and structural configurations found on individual properties and across communities. This approach enables accurate and cost-effective risk assessments tailored to the specific characteristics of each scenario, providing engineers with tools to evaluate the wildfire resilience of individual structures.

This study aims to evaluate the feasibility of using a high-fidelity, computational fluid dynamics (CFD)-based model as a performance assessment tool for individual properties in WUI fires. By recreating structure burning observed in Lahaina, Hawaii, the study seeks to identify gaps in knowledge and techniques related to modeling fire spread on a single structure and between neighboring residential buildings.

1.3 *Scope of Work*

The Maui wildfire has claimed 102 lives and decimated the historic Lahaina town, with thousands of acres burned and over 2,200 structures damaged or destroyed [1]. Strong winds, down-sloping coastal topography and lack of active fire suppression are key factors that contributed to the widespread devastation.

The structures shown in Figure 1 are those chosen for modeling in this study. The homes are located at 1259 and 1267 Nahale Pl, towards the northern end of Lahaina. These structures were burned completely during the wildfire. The structure at 1259 Nahale Place will be modeled using a high-fidelity simulation to capture fire propagation throughout the building accurately. The adjacent structure at 1267 Nahale Place will serve as the initial fire source for the burning of the 1259 one. A neighbor's security camera footage captured the entire fire as it developed in 1267 Nahale Pl and spread to 1259 Nahale Pl. The observable space in the security camera footage is shown in Figure 2. It has been estimated that the fire spread to 1267 Nahale Pl via the house adjoining its backyard. Due to the flames in the selected model area not being visible until they reach and ignite the exterior of 1267 Nahale Pl, the 1267 Nahale Pl becomes the point of fire origin within the simulation. There is not a considerable number of firebrands showering the area while 1267 burns and fires spread to the neighboring house, allowing models to ignore their influence without compromising accuracy.

The primary goal of this study is to replicate the fire at 1267 Nahale Pl and its spread to 1259 Nahale Pl. This replication will provide an appropriate fire source for the high-fidelity FDS model of 1259 Nahale Pl. Since the burning at 1267 Nahale Pl serves only as a fire source, the model does not require high fidelity, but it should accurately reproduce flame development.



Figure 1.1 Selected Model Area

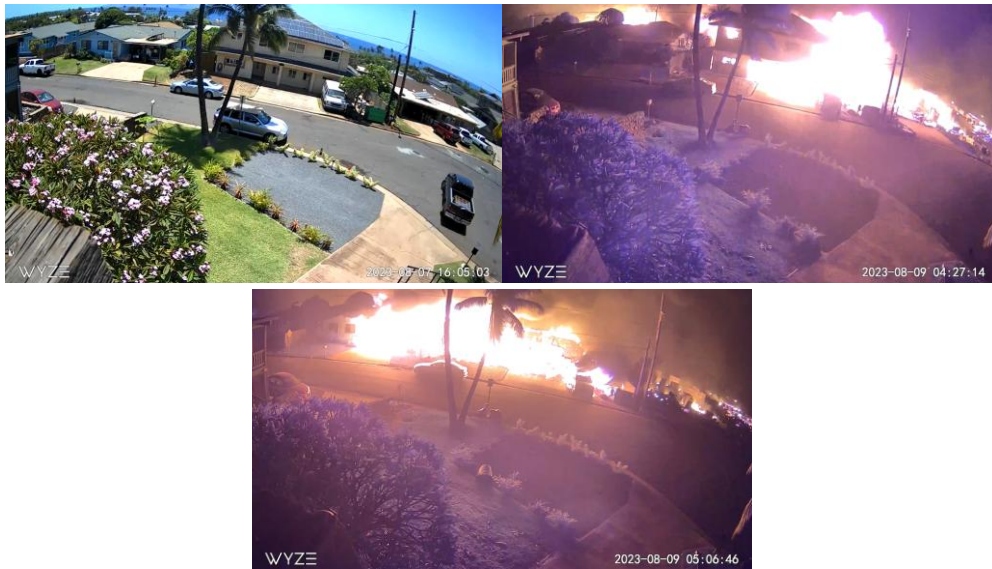


Figure 1.2 Security Camera Footage of 1267 and 1259 Nahale Pl

Chapter 2 Literature Review

Prior research has significantly advanced fire risk assessment in WUI communities, establishing a foundation for evaluating the application of CFD-based software in these contexts. This literature review examines prior efforts to advance understanding of WUI fire safety through full-scale experiments, identifies key fire-related phenomena that should be incorporated into computational models, and reviews validation studies of FDS for simulating these phenomena.

2.1 *Full Scale Testing*

2.1.1 Structure Separation in WUI Environments

Numerous experiments have investigated the influence of structure separation distance on fire dynamics in WUI settings. As this study aims to model ignition between adjacent structures in Lahaina, it is essential to understand how key parameters—such as wind speed and wall construction—affect fire behavior as a function of separation distance. This understanding is critical for developing accurate computational models for WUI fire scenarios.

A significant body of experimental work relevant to WUI fire risk assessment has been conducted by the National Institute of Standards and Technology (NIST). One series of experiments [3], performed in an outdoor setting, evaluated the thermal exposure from a burning shed to a target wall at separation distances ranging from 1.5 m to 4.5 m under various wind conditions. These experiments demonstrated that reducing the separation from 4.5 m to 3.0 m led to a threefold increase in heat flux and a doubling of peak temperatures. Notably, wind-driven convective heat transfer became dominant, as increased wind speeds suppressed the buoyant behavior of the fire plume.

In contrast, a separate series of indoor experiments [4], also conducted by NIST, used a similar shed and target wall configuration but excluded wind effects. In the absence of wind-driven heat transfer, even larger sheds had to be positioned closer to the target wall to produce significant thermal exposure. Given that the maximum separation distance tested in the outdoor experiments closely resembles typical spacing between structures in Lahaina, these findings underscore the necessity of accurately modeling wind effects to evaluate heat transfer and ignition risk between adjacent buildings at realistic separations.

An additional experiment conducted by NIST [5] investigated fire spread between adjacent structures with varying wall construction types at a fixed separation distance of 1.8 meters. This indoor study, performed without applied wind, compared ignition behavior between fire-resistant and non-fire-resistant target walls. Despite the close proximity of the structures, the fire-resistant wall did not ignite during the experiment. These findings further illustrate the complex interplay between structural materials, separation distance, and environmental conditions. Experiments conducted under varying wind conditions and construction types have produced contrasting outcomes, highlighting the influence of these factors on heat and mass transfer mechanisms. To accurately capture such effects in simulations, careful attention must be paid to mesh resolution and parameter selection, ensuring reliable predictions of ignition and fire spread between structures in WUI settings.

An experiment conducted by Japan's National Institute for Land and Infrastructure Management examined fire spread in densely built urban environments using a field of nineteen model homes at one-third the scale of typical Japanese residences [6]. Fire was initiated in a single structure, and spread was observed throughout the field. The model homes included a wood crib as the combustion source but lacked internal partitions such as walls and floors. In the first test,

poor compartmentation resulted in brief periods of fully developed fire and no spread to adjacent structures. In a subsequent test, galvanized steel shingles were used to reinforce the roofs. Both tests were conducted under low-wind conditions. Heat flux measurements indicated that radiative heat transfer was the dominant mechanism of flame spread in the absence of significant wind. While the experiment provided valuable insights into fire behavior in compact urban settings, its limited scalability to full-scale scenarios highlights the need for computational modeling to support risk assessment in real-world contexts.

2.1.2 Flame Spread from Environmental Sources

NIST has also conducted a series of experiments investigating fire spread from timber and vegetative fuel sources to representative structures. One such study [7] focused on the effects of wind-driven fire spread, examining both direct flame impingement and ember (firebrand) transport to target structures. The findings indicate that the accumulation of combustible materials significantly amplifies fire hazards in the downwind direction. Additionally, the likelihood of spot fire ignition on or near structures was strongly correlated with increased wind velocities. Based on these observations, the study recommends the implementation of non-combustible barriers between vegetative fuels and structures as a mitigation strategy, particularly to reduce the risk of wind-driven firebrand ignition.

2.2 Previous Modeling Efforts

Numerous studies have sought to model critical parameters associated with WUI fire events. Among the most significant phenomena when evaluating fire spread between adjacent structures are thermal exposure, ember accumulation, and the structural response to fire. Accurate

representation of these phenomena is essential for predicting ignition potential and understanding the dynamics of fire propagation in WUI environments.

2.2.1 Thermal Exposure in WUI Environments

WUI fires pose unique challenges due to the complex interplay between vegetation, structures, wind, and topography. Traditional fire risk assessments often rely on static representations of fire behavior, which may overlook critical dynamics influencing thermal exposure and ignition potential. Recent research has advanced both high-fidelity computational models, such as FDS and OpenFOAM, and simplified physics-based algorithms aimed at capturing these interactions more accurately. These approaches enable a deeper understanding of how fire propagates in WUI settings and offer tools for evaluating mitigation strategies, fuel management, and structural vulnerability with greater precision.

One study using OpenFOAM modeled wind-driven surface fires and their effects on an idealized cubic structure measuring $6 \times 6 \times 6 \text{ m}^3$ [8]. The study found that the presence of buildings significantly influenced the development of buoyant instabilities, which in turn affected fire plume behavior. These findings challenge traditional risk assessment approaches that rely on static fire representations, highlighting the importance of accounting for the transient and dynamic nature of fire propagation in estimating thermal exposure.

Thermal exposure resulting from interactions between structures and surrounding vegetation is a critical factor in WUI fire events. One study [9] examined three cases involving WUI dwellings surrounded by vegetative fuels compliant with local building codes, where fire behavior was replicated using FDS. Across all cases, the simulations demonstrated that FDS is capable of reasonably modeling flame-vegetation interactions, supporting its continued use in WUI fire risk assessments. However, the report notes that incorporating topographic effects and

wind conditions would improve model accuracy. Ongoing validation through physical experiments and refined computational modeling will be essential for evaluating the influence of vegetative fuel management strategies on fire risk in WUI settings.

FDS simulations operate on an orthogonal mesh, which presents challenges in accurately modeling vegetative fuels such as trees or shrubs due to their irregular geometry. To address this, particle-based fuel models can be used to represent complex vegetation as a cloud of thermally degradable particles. For example, Lagrangian particles have been used to model the burning of trees. These simulations were validated against NIST experiments on Douglas Fir tree burning by comparing the simulated and experimental mass loss rates [10]. Such models enable the simulation of energy exchange between fire and vegetation in cases where traditional grid-based geometry is inadequate.

In addition to thermal exposure from burning vegetation, structures in WUI environments are also vulnerable to heat transfer from nearby burning buildings. Accurately simulating fire spread between structures is therefore essential for capturing community-scale fire dynamics. As part of the verification and validation of FDS for WUI applications, a simulation conducted by NIST was replicated to compare numerical results with experimental data [11]. The experiment measured heat flux at targets placed at various distances from a source fire with a known heat release rate. The results from simulations showed strong agreement with the experimental findings, with a combined relative uncertainty of 5%, demonstrating FDS's capability for accurate fire simulations in WUI contexts. Such simulations offer critical insights for evaluating structure separation distances and informing code adaptations to better mitigate fire risk in densely built WUI areas.

Besides the use of CFD-based simulations, one study by NIST presents a simplified, physics-based algorithm to estimate the risk of structure ignition from burning vegetation in WUI areas, developed for integration into the USDA Forest Service's EcoSmart tool [12]. Using full-scale burn experiments of Douglas-fir trees, the study quantifies key fire behavior parameters (including flame height, heat release rate, and radiative heat flux), and uses them to construct a six-step model predicting whether thermal radiation from burning trees can ignite nearby structures. The model emphasizes ease of use and minimal data requirements, making it suitable for homeowners and planners, though it simplifies or omits factors like wind, embers, and time-dependent ignition, highlighting the need for further research to improve accuracy and applicability.

2.2.2 Ember Accumulation and Transport

High wind conditions, common in wildland and WUI fires, significantly contribute to ember generation and transport. Typically originating from vegetative fuels, embers can detach from flaming or pyrolyzing sources and ignite spot fires at considerable distances from the primary flame front, thereby amplifying fire spread and danger. A robust understanding of previous efforts to model ember behavior using CFD tools is essential for accurately simulating WUI fire dynamics.

One relevant model [13] examined ember accumulation on and around a typical WUI residence using FDS. The study conducted a parametric sensitivity analysis, varying fire and environmental inputs such as wind speed, ember mass flux, and roof surface roughness. Wind speed emerged as a particularly influential parameter: lower wind speeds were associated with increased ember accumulation on rooftops, while higher wind speeds shifted the risk to balconies and semi-enclosed areas. These findings underscore the need for detailed and accurate wind modeling in WUI risk assessments.

In another study [14], the authors simulated the burning of a single Douglas fir tree using the Fire Dynamics Simulator (FDS) to generate realistic fire-induced buoyant flow, but did not model ember (firebrand) generation directly from the burning tree. Instead, firebrands were manually injected into the simulation domain as Lagrangian particles based on mass, size, and distribution data obtained from NIST laboratory experiments. An inverse analysis was conducted to determine the initial velocities and directions of these particles to match experimental firebrand landing patterns. While the tree burning model captured heat release and buoyancy effects, the ember generation process was decoupled from combustion and implemented through externally prescribed particle inputs.

2.2.3 Structural Response

The structural response of buildings and their construction materials to heat and fire exposure is a critical factor in modeling flame spread between structures, particularly in WUI environments. A thorough understanding of structural response informs how buildings should be modeled in simulations to capture their evolving behavior under fire more accurately.

A study by De Beer [15] has developed an empirical firebrand pile heat flux model and also developed a numerical ignition model used to predict the ignition probability of an arbitrary target substrate when exposed to a glowing firebrand pile under wind. A dimensionless flame stability parameter was used as a material-independent criterion to characterize the ignition of a flammable substrate surface. Those models can be integrated into the FDS simulation to model the ignition of substrate by firebrand deposition in a probabilistic way, rather than directly simulating the transition of firebrand smoldering to active flaming on the flammable substrate surface and in a deterministic way.

A study by De Beer [10] developed an empirical model for the transient heat flux generated by glowing firebrand piles and a probabilistic numerical ignition model to predict the ignition probability of arbitrary combustible substrates exposed to such heat fluxes under wind. A dimensionless flame stability parameter was introduced as a material-independent ignition criterion, linking substrate thermal response to ignition probability. While these models are not currently implemented within FDS, they could be adapted to enhance firebrand ignition modeling in a probabilistic framework, offering an alternative to the deterministic threshold-based ignition criteria currently used in FDS.

Another critical event in fire development is window breakage. As flames spread within or between structures, windows often fail due to thermal stress. This change can intensify the fire within the original space and accelerate flame spread to adjacent compartments or neighboring structures by compromising the enclosure's integrity. In WUI fire scenarios, window breakage can also provide a pathway for embers to enter the interior of a structure, increasing the risk of ignition and interior fire growth. To improve the realism of such scenarios in fire simulations, experimental studies have proposed empirical criteria for window failure under fire exposure, such as critical surface temperature thresholds, which can be integrated into FDS models to better capture the response of glass in FDS [16–19]. However, the default radiation model in FDS—a gray “two-flux” approximation—has limitations when applied to spectrally dependent materials like glass. To address this, researchers have developed a spectral radiation heat transfer model based on the Spectral Discrete Ordinates Method (SDOM) [20, 21], which has been successfully implemented in FDS to simulate transient temperature distributions on window surfaces with greater accuracy. Building on these capabilities, FDS allows for the implementation of window failure using a

control logic driven by DEVCS-measured data, such as a predefined critical temperature threshold for glass failure [22].

Chapter 3 Introduction of Lahaina Fire and Choice of Model Area

In August 2023, a wildfire started on the western coast of Maui, devastating many communities throughout the island. The Maui wildfire has claimed 102 lives and decimated the historic Lahaina town, with thousands of acres burned and over 2,200 structures damaged or destroyed Click or tap here to enter text.[1, 23, 24]. Strong winds, down-sloping coastal topography and lack of active fire suppression are key factors that contributed to the widespread devastation. However, despite these factors, some buildings and building blocks survived the fire essentially undamaged [2]. It stands to reason that some construction features of those buildings, landscaping around their perimeters and/or their locations relative to other structures are responsible for their remarkable fire resistance. This chapter describes the factors contributing to the fire spread throughout Lahaina and identifies a specific area of the town that is to be recreated in FDS.

3.1 *Lahaina Wildfire*

3.1.1 Drivers of Rapid Fire Spread

Many factors of Lahaina's natural environment contributed to the extent at which the wildfire spread through the town. Among the most notable of these factors are the town's topography, the presence of vegetation intermingled with the build environment, and the dry, windy climate affecting Maui at the time of the fire.

The WUI is defined as the geographic area in which wildland vegetation contacts and interacts with human development. With Lahaina existing as a part of this area, it is natural that wildfires developing in nearby wild areas would continue to propagate towards adjacent vegetative areas. Much of the vegetation immediately adjacent to Lahaina comes from old sugar fields, which had not been maintained well since their closure decades before the fire [25]. Many of the plants

now found in these fields are not native to Hawaii; they were originally introduced for agricultural purposes and have since come to dominate the landscape following the closure of plantations. Many of the most invasive species of grasses found throughout the Hawaiian Islands are listed by the state's Department of Land and Natural Resources as having a moderate to high fire hazard [26]. The nonnative grasses were introduced specifically for their drought resistance, which has led to their rapid spread across parts of the islands during both rainy and dry seasons, when native plants may not spread as easily [27]. At the time of the fire, it was estimated that the highly flammable, invasive grasses covered a quarter of all land throughout the state of Hawaii [28]. With the effects of the invasive vegetation combined with native vegetation in the area, whether placed naturally or inserted by humans, there develops an environmental condition which allows fires to grow rapidly and strongly as it progresses to and through built environments throughout Lahaina.

Much of Maui's topography is marked by large dormant volcanoes which cause steep slopes throughout the island leading towards the coast. As winds flow across Maui and above the mountaintops, katabatic wind effects drive the air quickly downslope. Strong trade winds crossing the Hawaiian Islands combining with their mountainous terrain cause a strong funnel effect which crosses coastal towns. This funneling effect intensifies the typical fire hazards associated with high winds in WUI areas, making them especially severe in Lahaina.

While even the strong winds typical of West Maui would pose an increased fire risk to Lahaina, there were some environmental conditions occurring at the specific time of the fire which further increased the threat of a wildfire. At the time of the fire, Hurricane Dora was passing to the south of the islands, which climatologists credited for causing the high winds throughout Maui [28, 29]. However, a meteorological analysis conducted by NASA's Global Modeling and Assimilation Office (GMAO) found instead that Hurricane Dora was at too great a distance from

Maui for it to have affected the wildfires to a significant extent [30]. Instead, the analysis found that when comparing air pressure and wind speeds at the time of the fire, shown in Figure 3.1, with 23 prior years of historical data, there was an increase in wind speed and air pressure, and an overall shift in peak air pressure location towards Lahaina. Katabatic downslope winds caused by the high-pressure zone were funneled through gaps in Lahaina’s terrain, such as between areas with high vegetation density or through gaps between houses.

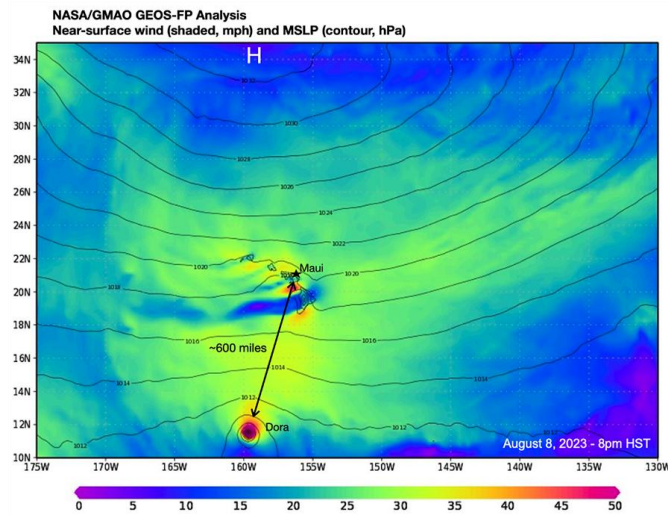


Figure 3.1 Lahaina Meteorological Conditions [30]

In addition to wind speeds, Maui was experiencing a drought in the weeks leading to the fire. During early summer 2023, Maui experienced a rapid two-category increase in drought severity, a pattern fitting that of an increasingly common phenomenon known as flash droughts [29, 31]. The drought causes a decrease in moisture content within vegetation throughout Lahaina, which is combined with drying effects from high winds.

An additional meteorological simulation created by NCAR [32] modeled the wind field over Lahaina at the time of the fire at a higher spatial and temporal resolution than that shown by the GMAO analysis publication. In addition to atmospheric simulation results, discussion of NCAR’s model identifies a key shortcoming in wildfire management technology, which keeps

emergency response in a reactive mode. It calls for the development of proactive risk assessment tools and the strengthening of faster-than-real-time, physics-based predictive capabilities. These analyses allow for quantitative examination of the environmental conditions surrounding the fire, however their more localized effects and interactions with the fire are not as apparent. The implications of the NCAR model outputs remain largely unaddressed when it comes to the localized impact of the environment on the dynamics of the fire at the neighborhood scale, and so the creation of a computational model to examine this impact would be very helpful for the purposes of risk assessment and management for properties and communities in the WUI.

3.1.2 Impact of the Wildfire to the Community

During the Maui wildfire, thousands of acres burned and thousands of structures were damaged or destroyed, as shown in Figure 3.2. In Lahaina alone, the Pacific Disaster Center (PDC) and the Federal Emergency Management Agency (FEMA) estimated that more than 2,200 buildings were destroyed [23, 24]. Most were residential, but the losses also included schools, businesses, public facilities, and numerous historic landmarks. The fire left entire neighborhoods in ruins and erased significant portions of Lahaina’s architectural heritage. Initial damage estimates reached nearly \$6 billion [33], and in September 2023 the U.S. Department of Commerce issued an official valuation of \$5.5 billion (2023 USD) [34]. One year after the incident, rebuilding costs for Lahaina and surrounding areas were projected to exceed \$12 billion [35].

The destruction triggered major population shifts, with many residents displaced and 370 fewer in-migrants than expected, reducing local spending and tax revenues by tens of millions annually. Thousands remain homeless, placing immense strain on Maui’s already limited housing infrastructure. Tourism—responsible for more than half of Maui’s jobs—faces serious gaps in infrastructure and staffing, while other sectors such as fishing are also reeling from fire-related

pollution and ongoing climate change impacts. Beyond economic and physical losses, the wildfire has deepened mental health challenges. Lahaina’s role as the first capital of the Hawaiian Kingdom and a cultural touchstone for Native Hawaiians means that its destruction represents not only a material loss but also a profound blow to community identity and heritage.



Figure 3.2 Damaged and Undamaged Structures in Lahaina [36–39]

Despite the widespread devastation, many structures survived among their destroyed neighbors, seeming essentially undamaged by the blaze. Much discussion has occurred about these structures and why they survived the wildfire. Possible factors include vegetation management, creation of fire-resistant barriers between surviving structures and their neighbors, and the use of fire-resistant materials in building construction [36]. Analysis of the impact of construction features seen in undamaged homes and how they specifically interacted with the progression and conditions of the fire helps to build an understanding of how to prevent the spread of fire to adjacent properties and structures. Development of engineering and risk assessment methods from such analyses will greatly help to mitigate losses and negative impacts brought about by fires in WUI communities. Recommendations for further action in preventing future devastating fires are

given in UL's *Lahaina Fire Forward Looking Report* [23]. Many of these recommendations are qualitative rather than quantitative in nature and are tailored specifically to Lahaina rather than WUI areas in general. Regardless, the report offers a basis for further action for risk mitigation, whose effectiveness and feasibility may be assessed through physical experiments and computational experiments. Quantitatively assessing these recommendations is of critical importance for ensuring that recommendations made to Lahaina and to other WUI communities do not absorb a potentially high amount of risk that would otherwise be mitigated through engineering analysis.

3.2 Selection of Model Area

3.2.1 Search for Viable Area

News, reports, text posts, videos, and photographs from multiple digital sources were analyzed to develop a timeline of wildfire events. Based on these data, a study area with comprehensive fire spread information was then selected for further analysis. The chosen area needed to be sufficiently large to support a representative model of WUI fire dynamics, yet small enough to remain within the computational constraints of FDS. Additionally, the presence of both destroyed and undamaged structures was required to enable simulation of varied structural outcomes and to analyze factors influencing fire transmission between buildings. This thesis focused on the analysis of burned structures. Future studies will also examine unburned structures to ensure that the simulation accurately captures both outcomes.

During the data collection process, a documentary created by Lahaina resident and firefighter Dan Nelson was identified. Nelson remained in the neighborhood longer than most residents, and a security camera on his home recorded footage of the fire's progression. Although many homes in the area were destroyed, his residence remained intact along with the security

camera footage. The footage captured by his security system provided a valuable record of fire behavior in the immediate vicinity. With Nelson's permission, this footage was used to develop a detailed model of the affected neighborhood.

3.2.2 Details of Selected Model Area

The structures shown in Figure 3.1 are those chosen for modeling. The homes are located at 1259 and 1267 Nahale Pl, towards the northern end of Lahaina. These structures were completely burned during the wildfire. The structure at 1259 Nahale Place will be modeled using a high-fidelity simulation to accurately capture fire propagation throughout the building. The adjacent structure at 1267 Nahale Place will serve as the initial fire source for the burning of the 1259 one. A neighbor's security camera footage captured the full duration of the fire as it developed in 1267 Nahale Pl and spread to 1259 Nahale Pl. The observable space in the security camera footage is shown in Figure 3.2. It has been estimated that the fire spread to 1267 Nahale Pl via the house adjoining its backyard. There is not a considerable number of firebrands showering the area while 1267 burns and fires spread to the neighboring house, allowing models to ignore their influence without compromising accuracy. The primary goal of this project stage is to replicate the fire at 1267 Nahale Pl and its spread to 1259 Nahale Pl. This replication will provide an appropriate fire source for the high-fidelity FDS model of 1259 Nahale Pl. Since the burning at 1267 Nahale Pl serves only as a fire source, the model does not require high fidelity, but it should accurately reproduce flame development. The replication of the flame development of 1267 Nahal Pl using FDS is the focus of this study.



Figure 3.3 Selected Model Area



Figure 3.4 Security Camera Footage

The security camera footage shown in Figure 3.4 gives a long, uninterrupted view of the area before and after the fire, as well as the growth of the fire through the houses themselves. 1267 Nahale Pl is the first chosen model house that ignites. The fire likely spread to this house from a neighbor which is not visible in the footage of the fire. This leads to an assumed ignition point of the back corner of the house, on the right side of this building. Within the footage, a third house on the far left of the frame can be seen, neighboring 1259 Nahale Pl (highlighted in a red frame in Figure 3.4). While flames spread in this direction through 1259 Nahale Pl and exposed this third house, it remained undamaged throughout the wildfire. Due to the scope of this project, however,

this house will not be included in modeling until subsequent efforts create a high-fidelity simulation of fire spread through 1259 Nahale Pl.

Maui county holds many documents related to building permits and renovation plans in the public record, available for access online. 1267's most recent major renovation was in 2006, which added the second story to the house. While drawings related to this renovation would have been very useful for creating the model of the house, digitization of records did not begin until 2009, and so the documents relating to the 2006 renovation unfortunately could not be found. However, a renovation in 2015 added solar panels to the roof of the second story, and the documents pertaining to this renovation have been digitized into the public record. These documents provide a scaled plan view of the house's second-story roof, which is useful for determining general exterior dimensions of the house for modeling. Additionally, 1267 Nahale Pl was most recently sold in 2019. The real-estate listings for this sale provide a general sense of interior contents and layout of the house in the absence of any footage inside of the house as the flames spread. The documents pertaining to the most recent renovation of 1259 Nahale Pl have been digitized into the public record and were used for reference when creating its geometry in FDS.

Chapter 4 Model Development using FDS

Models were created in the FDS software using the Pyrosim GUI for this research. The created models recreate the construction of the homes on Nahale Pl according to available knowledge from public record construction documents, real estate listings, common construction practice. Design fires have been created which recreate the estimated size and spread of the fire through 1267 Nahale Pl. Wind effects and vegetative fuels are modeled using established approaches from previous investigations of WUI fire dynamics. A mesh resolution sensitivity study was conducted to determine optimal cell size between houses.

4.1 Introduction of FDS

Computational fire modeling in this research is performed with the FDS software, version 6.9.1, developed by the National Institute of Standards and Technology (NIST). Results of model simulations are visualized using of the Smokeview software, version 6.9.1. An additional software developed by Thunderhead Engineering, Pyrosim, was used as a graphic user interface to aid with creation of FDS input files as well as viewing results.

FDS is a computational fluid dynamics model of fire-driven fluid flow. FDS numerically solves forms of the Navier-Stokes equations appropriate for low Mach Number ($Ma < 0.3$), thermally driven fluid flow, which are commonly seen in transport of smoke and heat from fires. The low Mach Number forms of the equations allow for simplistic numerical calculations that reduce computational cost without losing a significant amount of insight into physical processes pertaining to fire. It should be appreciated, however, that while the modified Navier-Stokes equations are valid for $Ma < 0.3$, the current validation of FDS only extends to $Ma \approx 0.1$. Governing equations solved in FDS are numerically solved through the use of second-order accurate finite

difference schemes, on a collection of three-dimensional grids with uniform spacing. By default, FDS lumps primitive species into fuel, air, and products, which only exist in the flow in certain proportions, and a single-step chemical reaction between the lumped species represents combustion. FDS solves the radiative transport equation using finite volume methods like the techniques used to solve equations for convective heat transport. Turbulence in flow computations is treated by means of Large Eddy Simulation (LES). The LES equations are derived by applying a low-pass filter to the equations for transport of mass, momentum, and energy. The filter width, Δ , is equivalent to the local cell size, δx , of the numerical grid defined for the simulation, a practice known as implicit filtering. Further information on numerical methods and governing equations used in FDS as well as their associated derivations can be found in the FDS technical reference guide [40].

The accuracy by which governing equations will be numerically solved is determined by the number of cells incorporated into the solution, which itself is limited by computational power. Parallel processing of FDS simulations may be used to increase computational power, allowing for more refined simulations to be run in shorter amounts of time. Parallel processing allows for allocation of a much greater amount of core processors for mesh assignment than in a typical commercially available desktop computer. The Zaratan high-performance computing (HPC) cluster provided by the UMD Division of Information Technology (accessible at <https://hpcc.umd.edu/hpcc/>) was utilized for parallel computing in this project. Within the Zaratan cluster, FDS makes use of Message Passing Interface (MPI) to compute each mesh as an MPI process. Individual cores may be assigned to make computations for singular large meshes, or alternatively assigned to multiple smaller meshes [41].

Verification and validation of FDS simulation results compared to measurements from a collection of experiments can be found in the FDS validation guide. The scope of this research is to analyze flame spread between exterior walls of residential structures in the WUI due primarily to radiative and convective heat transfer with the influence of high-velocity wind conditions. FDS has been validated against many previous experiments examining heat flux to walls and structure separation distances. Further details of these experiments are available in the FDS validation guide [11]. There are limited experiments detailed in the guide that help validate the capability of FDS to model structure fires with wind in a WUI setting. Consequently, limited previous attempts of examining feasibility of FDS as a risk assessment tool in these scenarios were found.

4.2 House Geometry and Construction

As described in Chapter 3, two model houses located at 1259 and 1267 Nahale Pl were carefully reconstructed in FDS to allow for accurate recreation of fire development and spread between structures. Geometry of these houses was recreated using recent renovation drawings, a space addition for 1259 Nahale Pl and a solar panel addition for 1267 Nahale Pl, available via Maui County Public Records. In addition, a third neighboring house located at 1266 Ainakea Rd was included in the FDS model to account for its potential disturbance to the local airflow, despite not being the primary focus of the simulation. This house's geometry was estimated from available satellite imagery and street views before the fire. The model of the three houses is shown in Figure 4.1. The materials and associated thickness used to construct the exterior walls were determined from available construction documents and typical exterior wall constructions which comply to applicable building codes in Maui County. The wall construction materials used in the model with their associated thicknesses, presented in order of outermost to innermost layer, are given in Table 4.1. Their thermal properties are given in Table 4.2.

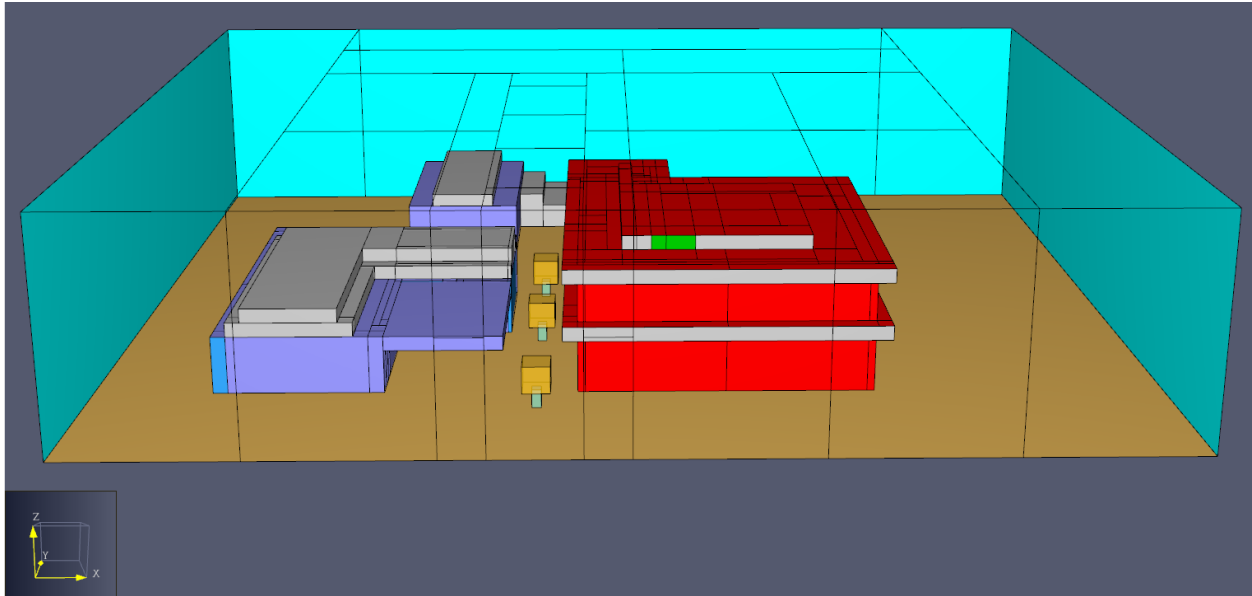


Figure 4.1 FDS Model Area

Table 4.1 Exterior Wall Materials

Layer	1259 Nahale PI	1267 Nahale PI
1 (Outermost)	Plywood, 0.0127 m [42]	Stucco, 0.0222 m [43]
2	HDPE, 0.0003 m [44]	HDPE, 0.0003 m [44]
3	OSB, 0.011 m [44]	OSB, 0.012 m [44]
4	Fiberglass Insulation, 0.1016 m [42]	Fiberglass Insulation, 0.1016 m [43]
5	HDPE, 0.0005 m [44]	Drywall, 0.1059 m [45]
6	Drywall, 0.0127 m [42]	N/A

Table 4.2 Material Properties

Material	Density, ρ (kg m^{-3})	Specific Heat, c ($\text{kJ kg}^{-1} \text{K}^{-1}$)	Thermal Conductivity, k ($\text{W m}^{-1} \text{K}^{-1}$)
Plywood	500 [46]	1.383 [46]	0.113 [46]
Stucco	2659 [47]	0.837 [47]	0.721 [47]
HDPE	940 [48]	2.3 [48]	0.4 [48]
OSB	664 [49, 50]	1.55 [49, 50]	0.13 [49, 50]
Fiberglass Insulation	12 [47]	0.84 [47]	0.04 [47]
Drywall	676 [51]	0.84 [51]	0.16 [51]
Asphalt Shingles	1219 [52]	1.025 [52]	0.14 [52]

Accurate specification of exterior wall construction is essential for modeling heat transfer into and through the walls of the houses. This is necessary to capture the thermal response of the wall assemblies, including surface temperature rise and heat penetration, which influence ignition potential and fire spread. Although the houses are modeled without interior partitions or furnishings, representing them as hollow enclosures allows for the evaluation of heat transfer through the exterior walls and the resulting temperature rise on their interior surfaces. This internal heating can contribute to delayed ignition and fire growth within the structure. Additionally, the heated exterior walls, particularly those of the two-story house, may re-radiate energy to nearby surfaces, affecting the surrounding thermal environment and potentially accelerating fire spread.

The roofs of both 1259 and 1267 Nahale Pl were also carefully reconstructed according to their original geometries. Solar panel renovation drawings created for 1267 Nahale Pl allow for reference when recreating the roof structure in FDS. Its roof was constructed on a 4/12 slope, which was reconstructed to align with FDS's orthogonal grid. For both homes, the roof structure

aligns with cubic cell sizes. The most recent real estate listing for 1267 Nahale Pl says that the outermost layer for the roof is made from asphalt shingles. These shingles cover a single layer of OSB as depicted in Figure 4.2. The roof is modeled as a layered surface, with an outermost 0.5 cm layer of shingles covering a 1 cm layer of OSB. Material properties for the shingles are obtained from FSRI’s material properties database [52]. The space past the thickness is left as empty space to allow for air temperature within the attic to increase. As seen in Figure 3.3, there exists not only the roof above the house’s second story, but also an overhang between the first and second stories, which is included in the FDS Model.

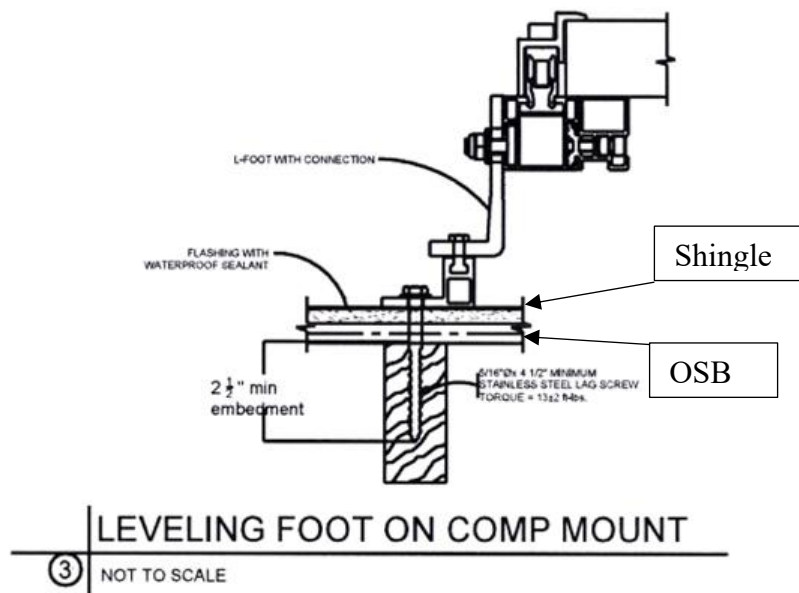


Figure 4.2 Roof Cross-Section [53]

4.3 Burner Configurations

1267 Nahale Pl acts as a fire source for the neighboring 1259 Nahale Pl. The source of flames coming from this house in FDS has been configured in several ways. These configurations differ in terms of the geometry and locations of the burners used to create flames in FDS. In two

configurations, burners extend across the full width of the exterior walls. In one, they span the full height of each story, while in the other (seen in Figure 4.1), they span the half height of each story. In the third configuration, burners are placed only at the window locations. This configuration exists because the house's exterior is made of noncombustible stucco and likely does not contribute much to heat transfer and flame geometry, while much of the flames can be seen coming out of the house's windows before the building enclosure fails under the fire. A fourth configuration has been created which models the burning not as exterior structure fires but rather as interior compartment fires, and enables heat to leave the house through openings placed at window locations. In the first three configurations, all burners are positioned vertically along the exterior walls, whereas in the interior configuration, the burners are positioned horizontally on the floor. Burner layouts for each configuration are shown in Figure 4.3. Burner surfaces are colored red by default in FDS, which was upheld in the model.

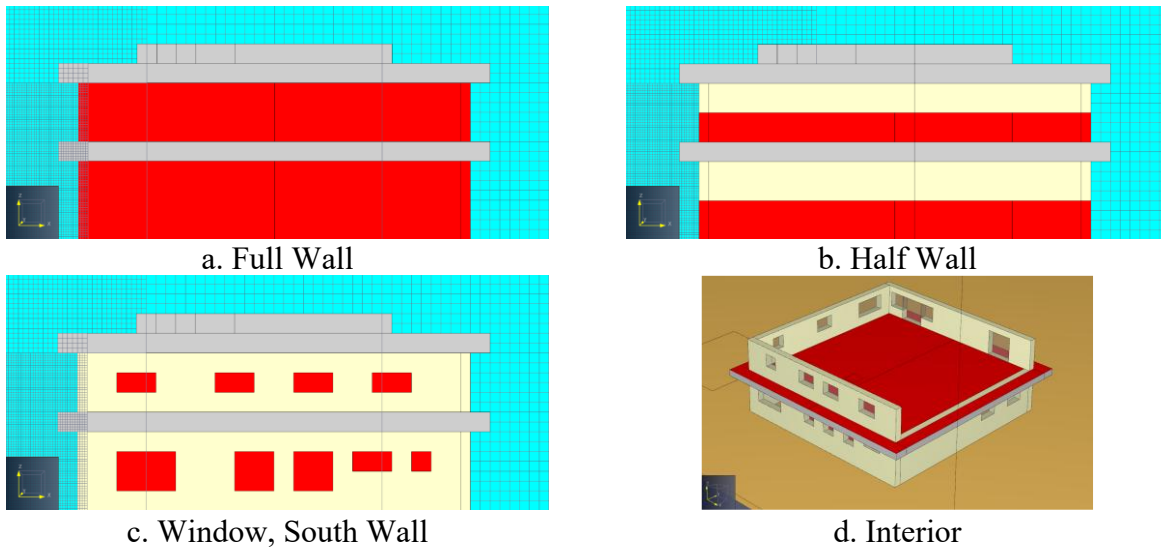


Figure 4.3 Wall Burner Locations (Burner surfaces are colored by red)

4.4 Design Fires for Level 1 and Level 2

Flames spreading through and out of 1267 Nahale Pl were modeled using a series of design fire curves. A design fire curve is assigned to each half of the floor, divided into a half closer to and further from the target wall of 1259 Nahale Pl. This results in two fires per floor, one on the side closest to 1259 Nahale Pl and one on the opposite side (henceforth referred to as regions 1 and 2, respectively), a total of four fires for the interior space of the house (the first and second stories). The growth rates and total duration of the design fires were estimated using the security camera footage of the fire. A previous study estimated fuel loads per unit area for different room types within Canadian residences [1]. Given that the residential building designs in the United States are largely similar to those in Canada, these fuel load densities were used to estimate the total fire load within 1267 Nahale Pl, based on the floor layout in the house's most recent real estate sale. In addition, the models consider the added fuel load from Douglas Fir wood framing throughout the house. The amount of wood used to frame the house's walls, floors, and ceilings was determined according to the size of the house estimated from renovation drawings [53]. The fuel load contributed by these members was based on the total mass of the wood in each region, following the procedure for mass-based wood fuel loads described in Section 4.5 of this report. In the FDS model, the design fire applied to a given house section has a uniform heat release rate with respect to the location. The heat release rate only changes with time, following the combustion model recommended by [2]. Growth times, burning duration, and fire loads for each design fire are given in Table 4.3. Here, the growth time refers to the interval between ignition and the attainment of steady state, while the burning duration denotes the total time the fire remains active.

Table 4.3 Design Fire Parameters

Region	Growth time (s)	Duration (s)	Fire Load (MJ)
Level 1, Region 1	487	3305	36561
Level 1, Region 2	367	3438	32604
Level 2, Region 1	109	2443	52972
Level 2, Region 2	297	2476	33005

Each design fire ignites at a different simulation time. The ignition of 1267 Nahale Pl is observed first on the back-right corner of its roof, as shown in Figure 4.4. This point is set as the start of the simulation.



Figure 4.4 1267 Nahale Pl Ignition Point

Ignition time of the interior space was determined as the time when flames became visible through the house's windows in that area. Ignition times after simulation start for each section are given in Table 4.4.

Table 4.4 Design Fire Ignition Times

Region	Ignition time (s)
Roof	0
Level 1, Region 1	585
Level 1, Region 2	291
Level 2, Region 1	980
Level 2, Region 2	844

Images corresponding to the time of ignition for each design fire, ordered from earliest to latest time of ignition, are shown in Figure 4.5. Within Figure 4.5, house regions are outlined in yellow, and indicators of the onset of burning are circled in red.



a. Level 1, Region 2



b. Level 1, Region 1



c. Level 2, Region 2



d. Level 2, Region 1

Figure 4.5 Design Fire Ignition Time

With the parameters for interior section design fires given in Table 4.3Table 4.4, the heat release rates applied to the wall burners in FDS can be determined. The design fire curves follow the method described in the SFPE Handbook of Fire Protection Engineering [51], in which the fire follows a profile with distinct growth, steady, and decay phases. A basic schematic profile is shown in Figure 4.6.

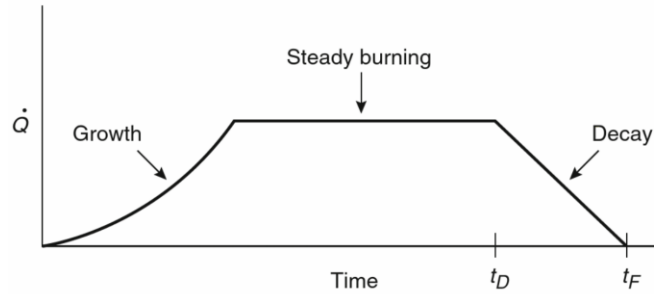


Figure 4.6 Design Fire Profile [51]

The HRR in the growth phase is proportional to the square of time after ignition during the growth phase, is constant in the steady phase, and linearly decreases in the decay phase. It is assumed that 30% of the total fuel load burns away in the decay phase. With these additional guidelines, the heat release rate over time can be determined with trivial integral calculus. The heat release rates used for the simulation are given in Figure 4.7.

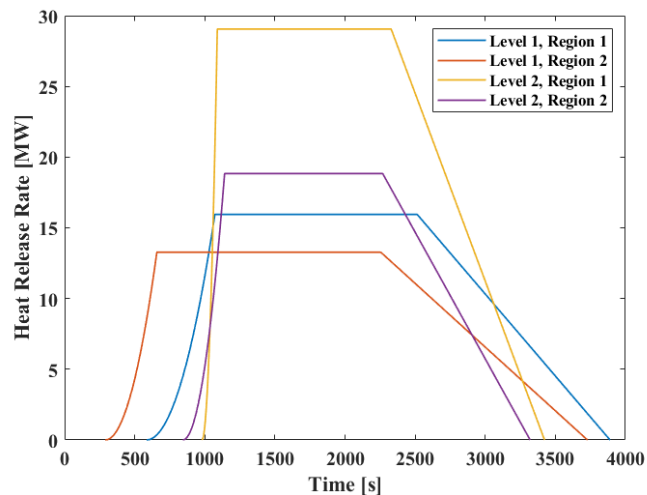


Figure 4.7 Heat Release Rates

The simulation continues to the point where all design fires are considered extinguished. At this point, no more significant amount of heat is being transferred from 1267 Nahale P1 to 1259 Nahale P1, and the exterior walls of 1259 Nahale P1 have been ignited into a self-sustaining flame. The image of the fire at the end of the simulation is shown in Figure 4.8.



Figure 4.8 Model End Time

4.5 Design Fires for Roof

In addition to design fires representing the fire load of the house for Levels 1 and 2, a design fire has been created for the attic and roof of the building. Two methods were examined to determine the size of the roof fire. The first method quantifies the fire load in the attic and roof based on the estimated surface area of exposed wood within the roof and attic, while the second method quantifies the fire load based on the estimated mass of wood used to construct the roof and attic. The first method, which follows the method used in NIST Technical Report 1838 [4], multiplies the exposed surface area of wood (including timber truss and OSB sheathing) by 50 kWm^{-2} , an experimentally obtained heat release rate per unit area [54], to calculate the heat release rate of the fire. Exposed surface area was estimated from the solar panel renovation drawings referenced in Section 0. In the second, mass-based method, the estimated mass is multiplied by the heat of combustion of wood to determine the fuel load. Surface sheathing is assumed to be made from OSB, which has a heat of combustion of 11.7 MJ kg^{-1} , taken from [49]. The wood frame members are assumed to be made from Douglas Fir wood, which has a heat of combustion of 14.7 MJ kg^{-1} , taken from [51]. Then, the fuel load is divided by the total duration for which the roof burns, yielding a heat release rate for the fire. In the simulation, roof and attic fires are assumed to be extinguished once structural collapse is observed in the video, assuming all fuel has been

consumed at the time of roof collapse. This is a simplification, as roof collapse does not necessarily indicate complete fuel consumption. As seen in Figure 3.3, there exists not only the roof above the house’s second story, but also an overhang between the first and second stories. As with the interior sections, the roof and the overhang have been divided into two halves, to account for differences in fire size caused by asymmetrical house geometry.

Table 4.5 shows the average heat release rates calculated by the mass-based and surface area-based estimation methods. Mass-based estimations of heat release rate were typically larger than surface area-based estimations, particularly for Level 2, Region 1. The conversion of the mass-based fuel load to its corresponding heat release rate assumes that all fuel in the roof burns from ignition until collapse. This assumption may not be entirely accurate and could partly explain why the mass-based heat release rate is higher than the surface area-based heat release rate. The surface area-based method allows for direct conversion of surface area to heat release rate, based on an experimentally obtained heat release rate per unit area. In this project, the surface area-based estimation was selected for the FDS model, as this method has been previously applied and validated in a well-documented FDS simulation similar to the one examined in this project [55].

Table 4.5 Roof Heat Release Rates

Section	HRR, Mass Basis (MW)	HRR, Area Basis (MW)
Level 1, Region 1	3.98	3.32
Level 1, Region 2	2.09	3.32
Level 2, Region 1	39.83	19.2
Level 2, Region 2	22.19	17.8

For simplification, the heat release rate of the roof fire was assumed to remain constant over time, as its growth phase could not be clearly identified from the camera footage, making it difficult to determine the fire growth rate. However, unlike the interior sections, the spread of the flames across the roof is clearly visible. The FDS model incorporates this spread by having the

roof design fire spread radially outward from the point of ignition at a constant rate as the simulation progresses, as shown in Figure 4.9. Flame spread in Figure 4.9 is illustrated through temperature increase outward from the point of ignition. The ignition point for roof fires is located at the back corner of the house, directly above Region 2. From the ignition point, the fire spread rate along the level 1 roof is 0.0112 m s^{-1} , and the fire spread rate along the level 2 roof is 0.0134 m s^{-1} . Fire spread rate is determined by estimating the time at which the fire reaches the corner of the roof opposite the point of ignition, and dividing the distance between these points by this estimated spread time.

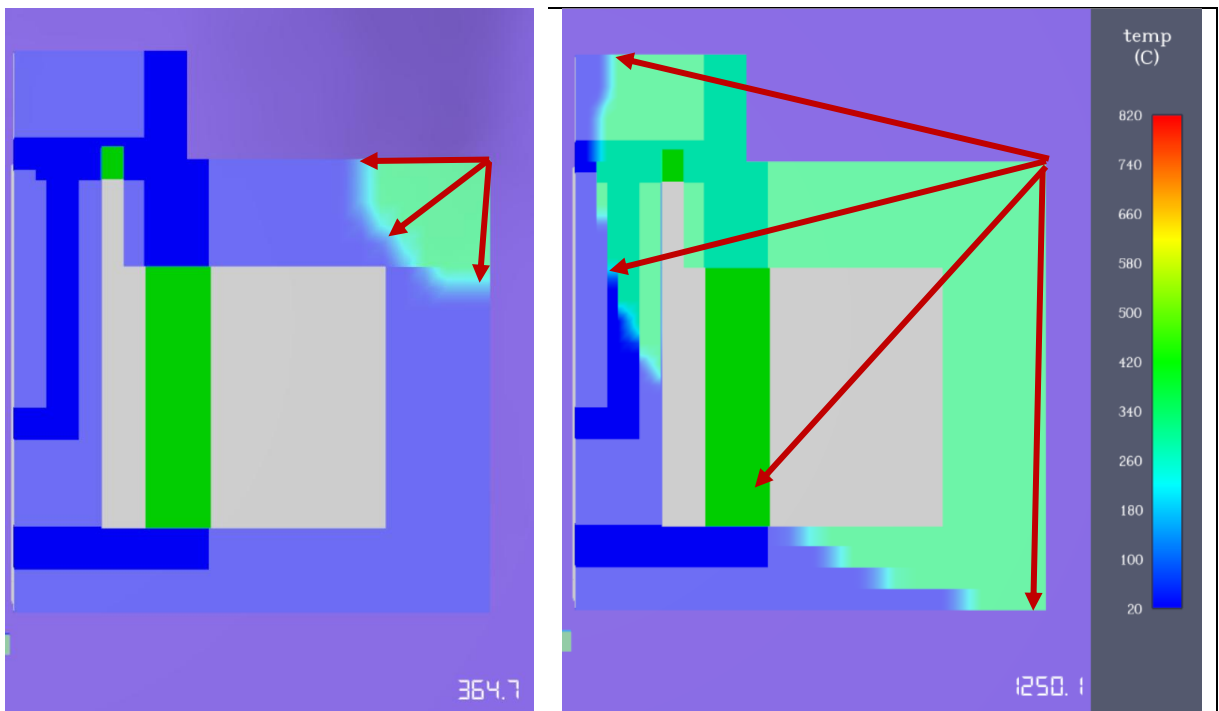


Figure 4.9 Roof Fire Spread

4.6 Wind Configuration

Wind is introduced into the model as a velocity boundary condition. Changes in velocity and direction are implemented via time-dependent ramps applied to the FDS wind namelist. The

National Center for Atmospheric Research (NCAR) simulated the wind field above Lahaina using the Weather Research and Forecasting (WRF) model [6]. The WRF model produced results on a 15-minute temporal resolution and 100m spatial resolution, which is rather coarse when considering the FDS simulation's runtime (67 minutes) and computational domain size (48 m x 51.2 m). The coarse temporal resolution would cause inaccurate results should the WRF model output be directly implemented into the FDS model. Instead, velocity values are interpolated using seven WRF results.

The fire duration is approximately 67 minutes and the temporal resolution of the outcomes from the WRF model is 15 minutes. This leads to the WRF model containing data at four times during the FDS simulation time, one shortly before, and two shortly after. The seven velocity points are interpolated with shape-preserving piecewise cubic interpolation of velocity over the desired temporal grid. This interpolation is performed using the “pchip” function in MATLAB. This yields an interpolated time-velocity function. WRF model results are interpolated onto a 50 second temporal grid. The interpolated function implemented into FDS along with the original WRF model results are shown in Figure 4.10.

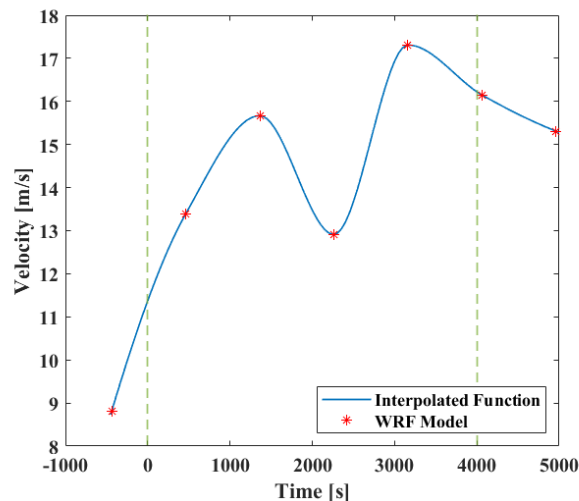


Figure 4.10 Time-Velocity Function

The variation of the wind direction throughout the FDS simulation for the neighborhood model was estimated from the security camera footage by observing the movement of smoke and vegetation. These directional changes were implemented at specific times corresponding to observed conditions rather than at uniform intervals. Direction of wind over time for the course of the simulation is shown in Figure 4.11. Note that the meteorological convention used in FDS is that an easterly wind has a direction of 90° and blows in the negative x direction, which in the case of this report's FDS models comes from the direction of 1267 Nahale Pl and blows towards 1259 Nahale Pl.

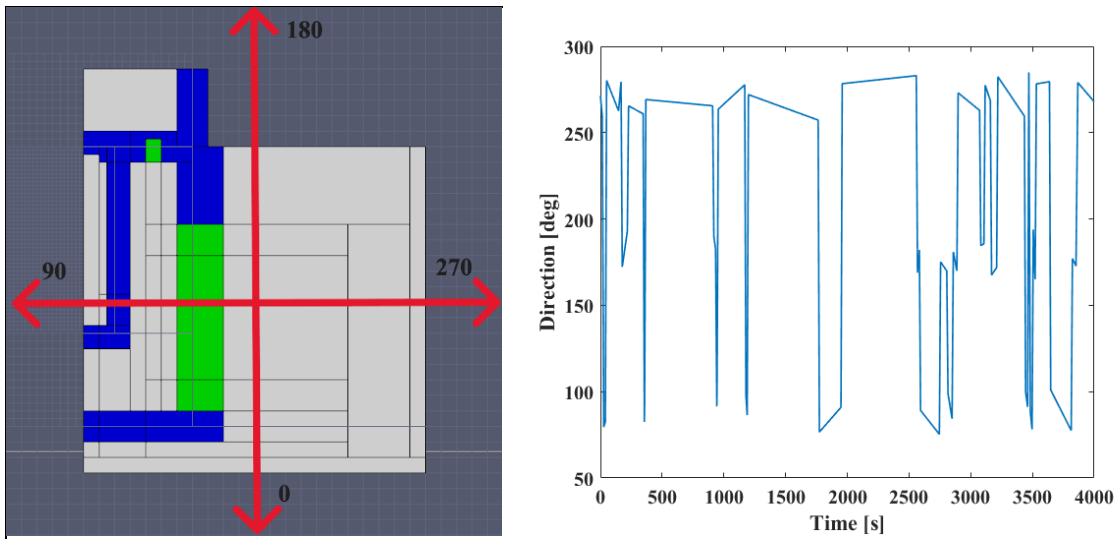


Figure 4.11 Wind Direction

4.7 Vegetative Fuels

The presence of vegetative fuels is a key contributor to the spread of fire in WUI settings, as they supply further fuel for fire and therefore heat towards surrounding structures. While structures such as 1267 and 1259 Nahale Pl could possibly be separated by a distance that prevents direct flame spread, the introduction of vegetative fuel sources may bridge these gaps by allowing flame

spread to closer combustibles. Between 1267 and 1259 Nahale Pl, there are three Plumeria trees, as shown in Figure 4.12. These trees can be seen burning during the fire, as shown in Figure 4.13.



Figure 4.12 Vegetation Between Houses



a. During Wildfire

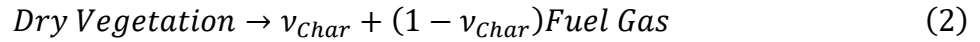
b. After Wildfire

Figure 4.13 Burning Vegetation

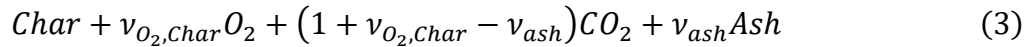
Methods for modeling vegetative fuel combustion are described in Chapter 17 of the FDS user guide [7]. Many of the methods described in this chapter of the user guide utilize a particle model, wherein vegetation is represented by a collection of particles that are heated via convection and radiation. FDS models solid-phase thermal degradation in response to the heating of these particles. This process is modeled with a sequence of three reactions. The first reaction is endothermic moisture evaporation:

$$\text{Wet Vegetation} \rightarrow v_{moist} \text{Moisture} + (1 - v_{moist}) \text{Dry Vegetation}; v_{moist} = \frac{M}{1 + M} \quad (1)$$

In this equation, M is the moisture fraction of the vegetation, determined on a dry weight basis. v_x is the stoichiometric coefficient of a given species, x . The second reaction is endothermic pyrolysis of dry vegetation:



The final reaction is exothermic char oxidation:



The FDS verification and validation repository on GitHub contains inputs for several simulations used to validate vegetative combustion in FDS for use in wildland fire modeling. A particularly useful model aimed to recreate a NIST experiment in which a Douglas Fir tree was burned. The trees used for physical experimentation and recreated through numerical modeling in FDS varied primarily in their moisture content. Comparative results of heat flux measurements, averaged for vertical arrays placed 2 m and 3 m from the burning tree, are shown in Figure 4.14 [11].

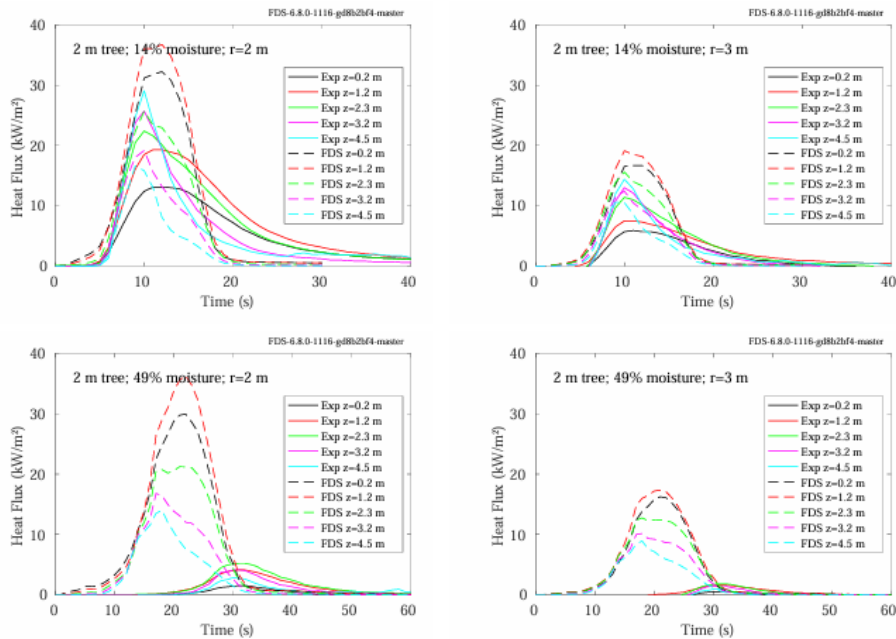


Figure 4.14 Douglas Fir FDS Validation [11]

Greater disparity between experimental and numerical results is seen for trees with higher moisture content, where heat fluxes computed by FDS are overestimated as compared to the results of the experiments. However, as mentioned in *[Weather Conditions]*, Lahaina was experiencing a significant drought for much of the time preceding the wildfire, and as such, using vegetative fuel sources with lower moisture content would yield more appropriate and accurate results.

The trees used for the validation models are Douglas Fir trees, while the trees present in the model area are Plumeria Trees. Although Douglas Fir and Plumeria trees would likely have different properties in terms of geometry, foliage density, and overall combustion properties such as char yields and heat of combustion, no specific properties could be found for plumeria trees. Consequently, the Douglas Fir tree validation model, which has fully defined combustion parameters according to Equations (1)-(3), has been implemented into the Lahaina FDS model. The geometry of the particle groups has been adjusted to match estimated geometries of the Plumeria Trees.

The tree model uses four types of cylindrical particles to represent branches and foliage in the tree. These vary in their length and surface area to volume ratio. Properties for each particle type are given in Table 4.6.

Particle	Length (m)	Surface Area to Volume Ratio
Foliage	0.2	3940
Small Roundwood	0.1	2667
Medium Roundwood	0.1	888
Large Roundwood	0.14	500

In the validation model, these particles are implemented on a 10 cm mesh grid, with a density of one particle per cell. This density may be adjusted for implementation into the Lahaina

model should other grid resolutions be used at tree locations. Further discussion of grid resolution and its impact on vegetative fuel modeling is contained in Section 4.9.

4.8 Radiation Solver

FDS uses the radiative transport equation (RTE) to model thermal radiation. The RTE accounts for emission of radiation by hot gases and surfaces, absorption of radiation by participating media, scattering of radiative heat, and transmission through semi-transparent media. FDS discretizes the radiative spectrum into a number (N) of bands, with a separate RTE derived for each band. The radiation intensity, I , at a given location x is given by:

$$s \cdot \nabla I_n(x, s) = B_n(x) - \kappa_n(x)I_n(x, s), \quad n = 1 \dots N \quad (4)$$

$$I(x, s) = \sum_{n=1}^N I_n(x, s) \quad (5)$$

In Eq. (4) above, $B_n(x)$ is the emission source term, and $\kappa_n(x)I_n(x, s)$ defines energy loss by absorption. s represents the direction vector for a given band.

In most large-scale fire scenarios, soot is the most important combustion product, controlling thermal radiation from fire and hot smoke. Soot has a continuous radiation spectrum, and as such FDS assumes that the gas behaves as a gray medium. Spectral dependence is lumped into a single absorption coefficient, with the radiation source term I_b at location x given by Eq. (6) for blackbody radiation intensity:

$$I_b(x) = \frac{\sigma T(x)^4}{\pi} \quad (6)$$

where σ is the Stefan-Boltzmann constant, and $T(x)$ is the temperature at a given location x .

Compared to the size of the flame sheet, the numerical grid used in FDS tends to be relatively coarse. The source term in Eq. (6) is dependent on flame temperature to the fourth power, however the flame sheet is typically not well-resolved on the numerical grid. Consequently, the source term in the RTE cannot be reliably calculated. As an alternative, the radiative fraction,

χ_r , may be explicitly defined for a reaction, representing the portion of a fire's heat release rate emitted as thermal radiation. The radiative fraction is given a default value corresponding to the reaction fuel; however, the value may be manually reconfigured by users as needed.

By default, FDS implements an optically thick radiation model with a defined background concentration of carbon dioxide and water vapor. The default relative humidity, which introduces water vapor, is 40%. The default ambient mass fraction of CO₂ is 5.95×10^{-4} . These parameters may be adjusted by the user as necessary. Although CO₂ and H₂O absorb thermal radiation from fire, they participate only in a relatively narrow spectral band. The gray gas assumption used in FDS smears the spectral absorption, and as such the thermal radiation absorbed by CO₂ and H₂O is overestimated by the numerical calculations as compared to physical reality. Background CO₂ concentration and relative humidity may both be set to zero, ignoring this absorption and ridding the simulation of the overestimation.

An additional important consideration for radiative heat transfer calculations in FDS is the radiative path length. Thermal radiation has a range of wavelengths absorbed by each component of the medium through which heat is transferred, and each wavelength has its unique absorption coefficient. The gray gas assumption used by FDS assumes only one absorption coefficient, which is a combination of all values. To calculate this effective coefficient, FDS uses a particular path length, L , which is the distance over which the effective absorption coefficient is optimum. The effective absorption coefficient is calculated as a function of the total radiation source term (I_{tot}), blackbody radiation source term (I_b), blackbody radiator temperature (T) and effective temperature of flame radiation (T_{rad}) with the equation:

$$\kappa = -\frac{1}{L} \ln \ln \left(\frac{I_{tot} - I_b(T)}{I_b(T_{rad}) - I_b(T)} \right) \quad (7)$$

By increasing the path length in Eq. (7), the effective absorption coefficient, and therefore the overall absorption predicted by the model as calculated in Eq. (4) will decrease. The default path length in FDS is 10 cm. There will typically not be a single path length which will yield a correct heat flux both near and far from the fire. To measure heat transfer to a target surface, it is typically recommended that the path length is set to the distance between the flaming source and the target surface. In the context of the Lahaina model, this path length would be the structure separation distance, 4.4 m.

One option within FDS is to configure the fire such that it is considered optically thin. In this case, reabsorption of thermal radiation by all gases is neglected. The fire will radiate a predetermined amount of radiative energy, specified by χ_r , which is transported towards the domain boundaries without reabsorption by colder gases. In WUI settings, reabsorption of thermal radiation may be difficult to predict and may ultimately be grid-dependent. By setting the fire as optically thin, the absorption term κ in Eq. (7) will be set to zero, and the fire will radiate the fraction of energy given by χ_r without the calculation of reabsorption by products of combustion or surrounding gases. In this mode, the results remain the same regardless of the background gas concentration or the path length.

A small test simulation was created to examine the impact of these parameters on radiative heat transfer with the separation distance between houses seen in Figure 4.1. The simulation layout is shown in Figure 4.15.

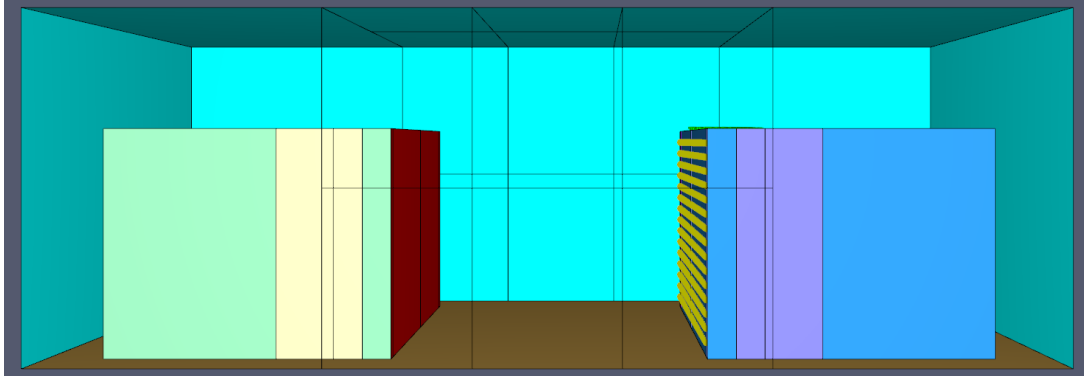


Figure 4.15 Radiation Configuration Test Simulation

This simulation placed a flaming surface with the heat release rate per unit area corresponding to the peak HRRPUA in the full wall configuration for Level 1, Region 1. Devices were placed along the target wall surface to measure heat flux with different configurations. The test considered a configuration with all radiation parameters kept as their default (background CO₂ and H₂O included, 10 cm path length), two configurations without background CO₂ and H₂O (one with a 10 cm path length and the other with a 4.4 m path length), and a fourth configuration with the optically thin model enabled. Results from this test case are given in Figure 4.16.

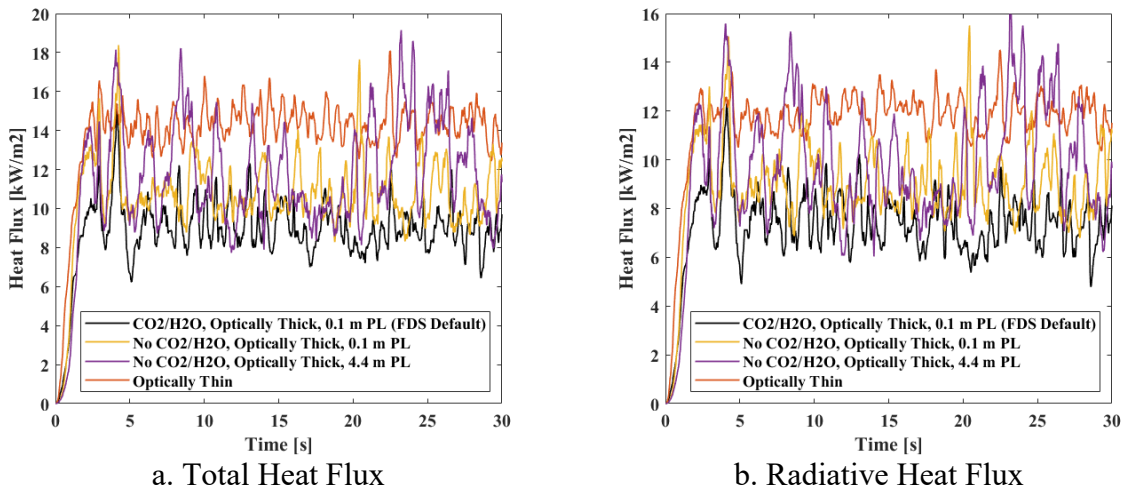


Figure 4.16 Radiation Parameter Tests (Optically thin selected)

In the optically thick mode, measured heat fluxes increased when background water vapor and carbon dioxide were removed from the simulation. The heat flux over time data with

background gases removed is relatively noisy, so it becomes difficult to ascertain the exact impact of adjusting radiative path lengths. Conversely, noise is relatively low in the simulation with background gases.

In FDS, the default gray-gas radiation model accounts for emission and absorption by participating media, with soot typically the dominant contributor in fires. For scenarios that are plausibly optically thin, for example, open-air flames with low soot yields and clear line-of-sight to targets, one may set `OPTICALLY_THIN=T`, which neglects reabsorption by gases and soot and enforces the user-specified radiative fraction. For the scenario simulated in this project, we used the optically thin radiation model, which increases the predicted heat flux on the exterior walls of the target building and brings the simulated ignition time closer to that observed in the video. With the optically thin mode selected, the results are unaffected by whether background water vapor or carbon dioxide are included, and are also independent of the path length. However, this choice warrants further discussion in future work.

To ensure appropriate spatial accuracy, the number of radiation angles may be increased from its default of 100 to increase the angular resolution of spatial discretization of the RTE. Studies on the requirements for accurate angular resolution [8] indicate that the number of radiation angles necessary to accurately resolve a target at a separation distance H , given an emission source surface area S , can be estimated using the following equation:

$$NRA = N_{\Omega} \frac{4\pi H^2}{S} \quad (8)$$

A separation distance of 4.4 m and a surface area corresponding to the total western wall burner surface area for each respective configuration (as shown in Figure 4.3) were used to calculate NRA values. For the interior burner configuration shown in Figure 4.3d, a surface area equal to the total window opening area along the wall was used. Evaluating the number of radiation

angles required according to Eq. (8) shows that the required angles for the full wall, half wall, and window (and, equivalently, interior) configurations require a minimum 12, 24, and 91 radiation angles, respectively. This shows that the default 100 radiation angles used by FDS is sufficient for all configurations.

4.9 Computational Domain

The definition of the computational domain is a critical component of any FDS simulation, as it establishes the physical boundaries within which fire and fluid dynamics are modeled. An appropriately defined domain ensures that all relevant thermal and physical phenomena are captured with sufficient accuracy while minimizing unnecessary increases to computational cost. Equally as important as domain size is the resolution of cells within the domain. Fine mesh resolution is essential for accurately capturing key phenomena such as flame impingement, radiant heat transfer between structures, and the flow of hot gases and embers through narrow gaps or around architectural features. In WUI scenarios, insufficient resolution may smear thermal gradients and underpredict critical behaviors like ignition of siding materials or window breakage. However, finer resolution significantly increases computational cost, making it important to strategically refine the mesh in areas of interest while maintaining coarser cells elsewhere to optimize performance.

4.9.1 Domain Boundaries

The computational domain boundaries were positioned to ensure that heat development within the domain was unaffected by boundary effects, and that boundary conditions, such as wind, could fully develop before interacting with the model geometry. Expanding the boundaries of the computational domain was performed with two different tests. The first test was intended to ensure

that flame extension away from the 1267 Nahale PI model would not reach the boundary of the computational domain. This was conducted simply by placing the model of 1267 Nahale PI within an otherwise empty computational domain, which was constructed on a uniform, relatively coarse 0.5 m grid. Roof and wall burner heat release rates were set to their maximum value, corresponding to the steady state phase of the design fire shown in Figure 4.7. Wind directions were varied, with the velocity being equal to the maximum value used in the duration of the model according to Figure 4.10. The second test was intended to ensure that wind velocities could develop properly to their prescribed value when introduced at the simulation boundary before interaction with model geometry. This test involved creating an empty computational domain on a 0.8 m grid, as shown in Figure 4.17.

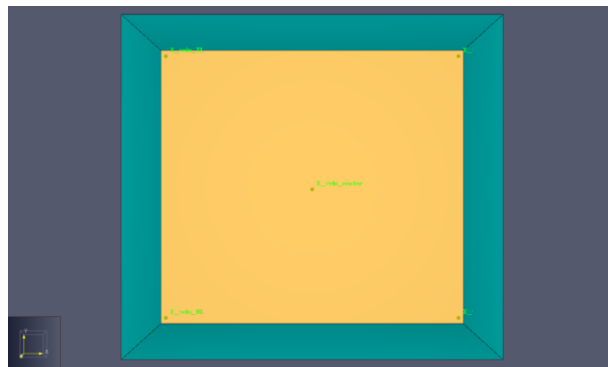


Figure 4.17 Wind Development Model

Within the domain, 10 devices are placed, two at each corner and two more at the center of the computational domain, which measure the x and y components of velocity at each location. Velocity is introduced at domain boundaries using the same procedure described in Section 4.6. Wind is introduced at all angles, making a full clockwise rotation starting from 0° , following the convention shown in Figure 4.11. The wind rotates clockwise at a constant rate, before returning to its starting position at the end of the simulation. This test showed that wind velocity profiles established rapidly after being introduced at the computational domain boundaries, indicating that

it was unnecessary to place the domain boundaries a significant distance away from the model geometry. Results for this test are given in Figure 4.18.

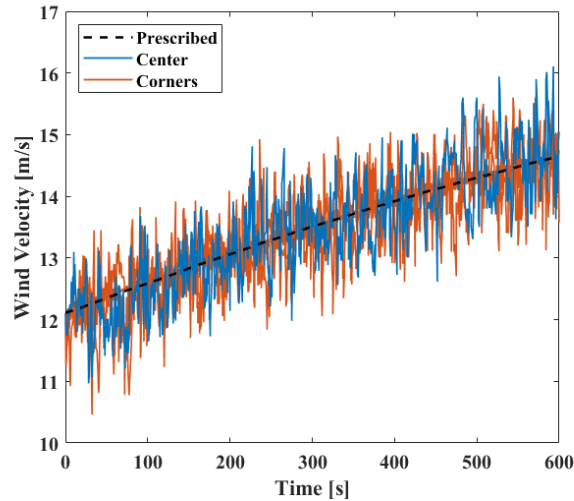


Figure 4.18 Wind Velocity Development Test Results

With the above tests performed, a final computational domain size of 52 m in the x-direction, 44.8 m in the y-direction, and 12.8 m in the z-direction was created and determined to be appropriate for use in the simulation.

4.9.2 Grid Resolution

Mesh sensitivity analysis is the process of systematically varying the computational mesh resolution to evaluate how sensitive key simulation outputs are to changes in cell size. This analysis is essential to ensure that the model accurately resolves the physical phenomena of interest without introducing significant numerical artifacts or excessive computational cost. In the context of flame spread between structures in WUI settings, mesh sensitivity is particularly important because the interaction between fire plumes, radiation, and complex building geometries can be highly localized and dependent on fine-scale thermal and flow gradients. By comparing results such as heat flux, surface temperature, or time to ignition across different mesh resolutions, it is possible

to determine whether the chosen mesh adequately captures critical fire dynamics and whether further refinement is needed in key regions. This process helps build confidence in the simulation results and ensures that conclusions drawn from the model are not unduly influenced by numerical discretization.

Similar to the tests described in Section 4.9.1, a simplified geometry model was created to test the convergence of key results as the grid cell size was reduced, as shown in Figure 4.19. The simplified model contains the same house geometries as in the full model shown in Figure 4.1. The roof geometries of 1267 Nahale Pl and 1259 Nahale Pl (right and left sides of Figure 4.19, respectively) are omitted from the mesh sensitivity model for simplicity. A tree constructed according to the parameters described in Section 4.6 is included in the mesh sensitivity model to ensure that the convergence study results consider the impact of vegetative fuels. Structures in the simplified model are constructed following the process described in Section 0, with the design fire only applied to the exterior walls of 1267 Nahale Pl, corresponding to the steady state HRR for Level 1, Region 1, and Level 2, Region 1, shown in Figure 4.7.

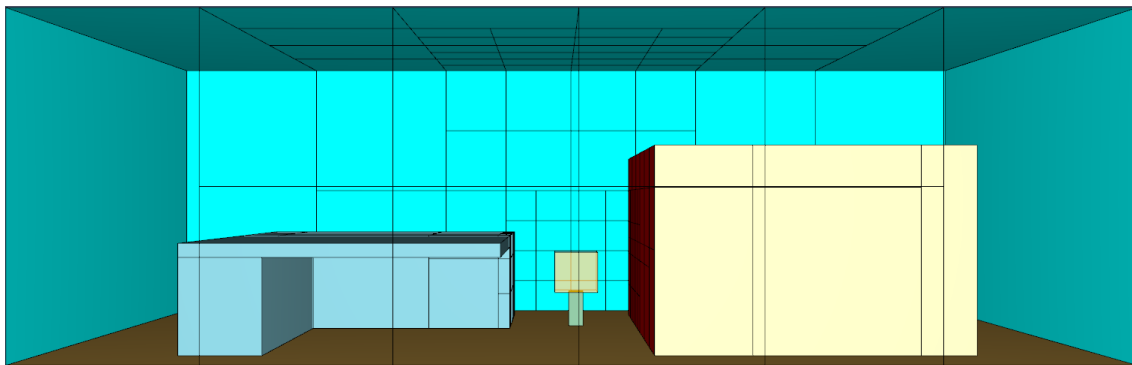


Figure 4.19 Simplified Model for Mesh Sensitivity Studies

Convergence tests were performed in the simplified models with a minimum cell size of 5, 10, 20, and 40 cm, henceforth referred to as the 5 cm model, 10 cm model, 20 cm model, and 40 cm model, respectively. The sensitivity model examines only the space between the houses, and

removes the rest of the full model's computational domain to increase speed and reduce cost of computations. The smallest cells in the simplified model are placed in the space between structures, normal to the exterior wall of 1259 Nahale Pl which faces 1267 Nahale Pl. An example using the 5 cm model is given in Figure 4.20. Note that the ratio of mesh sizes between adjacent regions is maintained at no more than 2:1. (i.e., 5 cm meshes are adjacent to meshes with resolutions no greater than 10 cm, and so forth) to ensure accurate information transfer and minimize error across adjacent meshes with unequal cell resolutions.

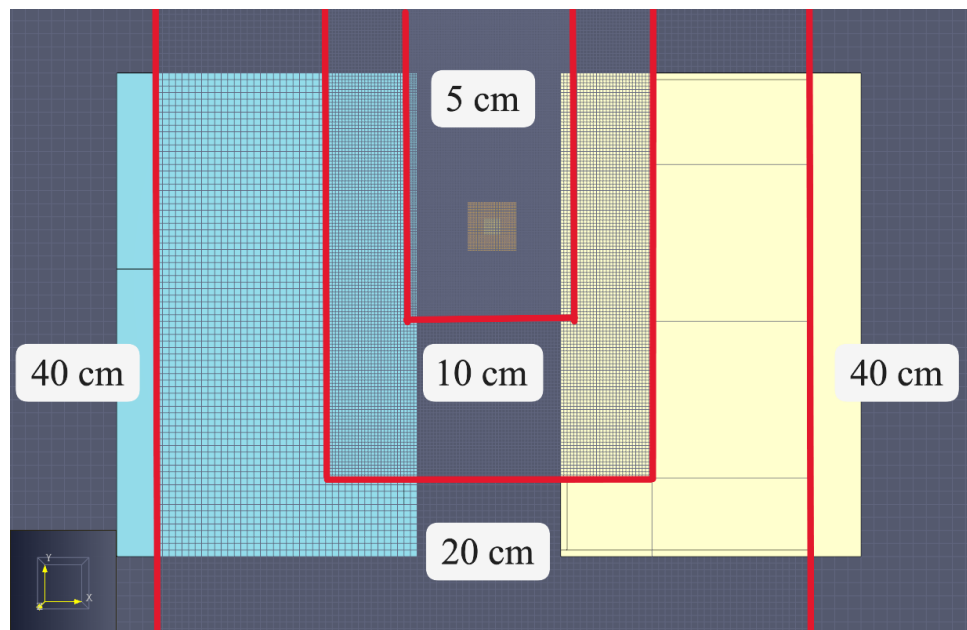


Figure 4.20 Example of Grid Alignment in the Simplified Model (with a minimum cell size of 5 cm)

To improve computational efficiency, the computational domain of the sensitivity test models was split into multiple smaller meshes, computed in parallel with Message Passing Interface (MPI). Further discussion of MPI and its applications to FDS modeling can be found in Section 4.8.3 of this report. Each mesh within the sensitivity study contains roughly the same number of cells to ensure load balancing. The 5, 10, and 20 cm models contained approximately

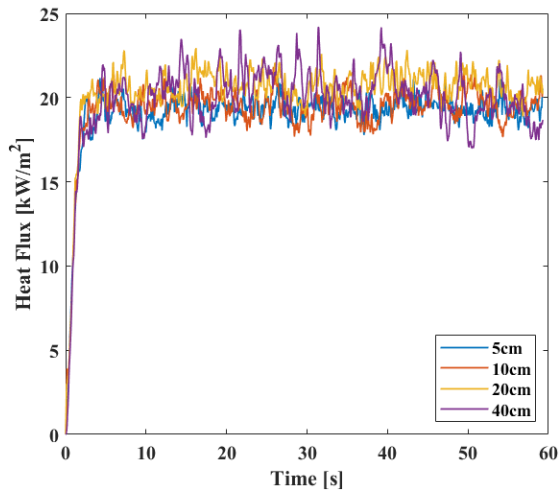
15,000 cells per mesh, and the 40 cm model contained approximately 14,600 cells per mesh. The total number of meshes used in each simulation is given in Table 4.7.

Table 4.7 Mesh Sensitivity Model Mesh Count

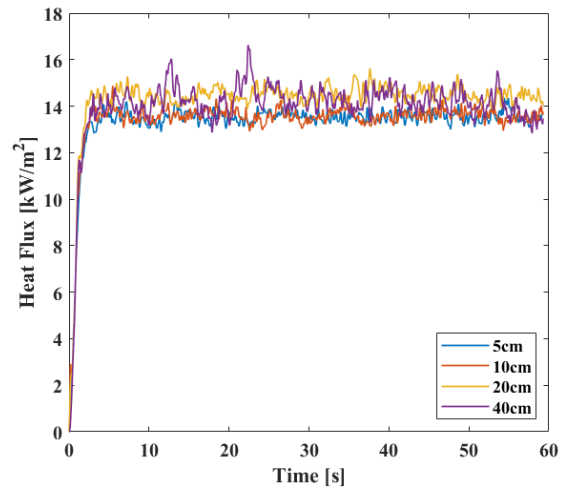
Smallest Cell Size (cm)	Number of Meshes
5	230
10	26
20	12
40	5

Despite relatively equal cell count per mesh across all models, the runtime of the mesh sensitivity models tended to increase as cell size decreased. The model with only 40 cm cells required only 45 minutes of wall time to complete, while the most refined model with 5 cm cells required 8 hours of wall time. FDS implements the Courant-Friedrichs-Lewy (CFL) constraint for simulation stability. Physically, the constraint states that a fluid and the information associated with it, such as heat, must not traverse more than one cell length in a single time step. When cell size is decreased, the time step required to adhere to the CFL constraint also decreases, yielding longer runtimes despite maintaining computational load per step.

An array of devices was placed on the exterior wall of 1259 Nahale Pl closest to the flames to collect heat transfer data and compare across models with different grid resolutions. The model measures incident heat flux and radiative heat flux at the target wall as well as the exterior surface temperature of the target wall. The spacing of devices measuring relevant quantities is equal to the finest cell size in the model, as devices are located at the point of intersection between cells. Model results for maximum and average values of total heat flux, radiative heat flux, and wall temperature are given in Figure 4.21 through Figure 4.23.

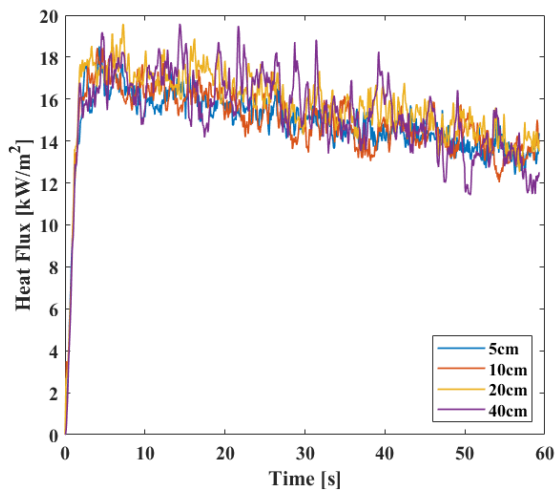


a. Maximum Value Measured

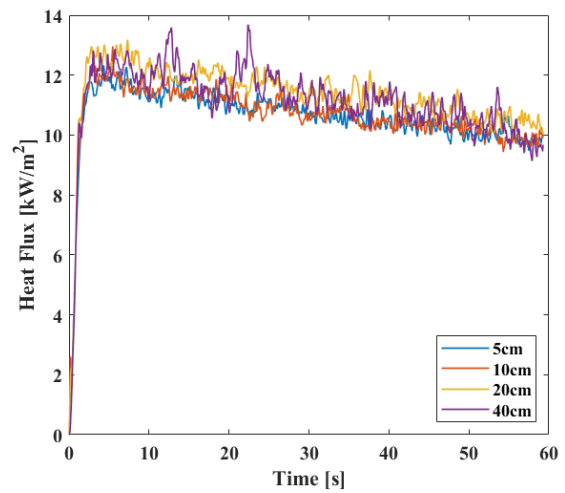


b. Average Value Measured

Figure 4.21 Total Heat Flux at Target Wall

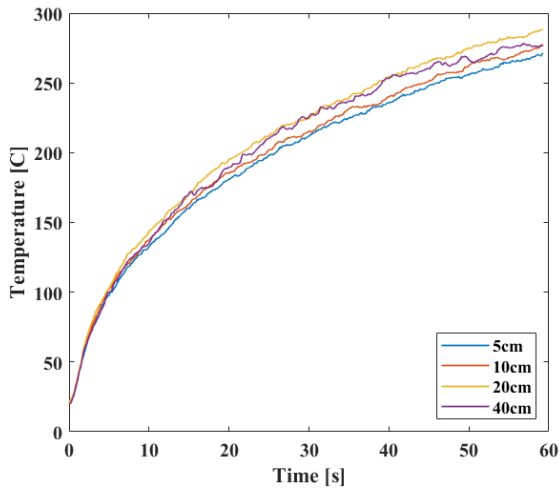


a. Maximum Value Measured

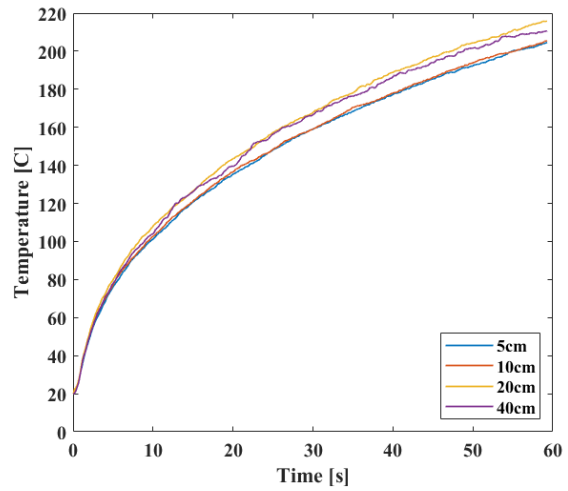


b. Average Value Measured

Figure 4.22 Radiative Heat Flux at Target Wall



a. Maximum Value Measured



b. Average Value Measured

Figure 4.23 Target Wall Surface Temperature

Data for heat flux is rather noisy, and thus it can be difficult to determine specific trends between models with different cell resolutions. However, close inspection shows that there is a slight increase in values measured at 20 and 40 cm grid resolutions as compared to those measured at 5 and 10 cm grid resolutions. This difference becomes slightly apparent for the measured wall surface temperature values, particularly for the average values seen in Figure 4.23b. The average temperatures measured for the 5 and 10 cm models are near identical for the duration of the simulation, meanwhile there is a slight increase (less than 10%) in the measured surface temperature for the 20 cm and 40 cm models compared to their more refined counterparts.

4.9.3 As the measured values for 5 and 10 cm models are close to identical for surface temperature, which will ultimately be a key parameter for exterior wall ignition time, there is little benefit gained for the associated computational cost increase when refining the model from 10 cm cells to 5 cm cells. Additionally, a problem is introduced when modeling vegetative fuels at resolutions smaller than 10 cm, as the particle sizes obtained from the validation model must be adjusted to fit within a single cell and maintain density of vegetation across the tree. Consequently, it was determined that a 10 cm resolution should be used for the most refined grid cells within the computational domain for the full-scale model.

Final Computational Domain

With the mesh sensitivity study finalized, a mesh grid may be created which aligns to the geometry needed to model the houses on Nahale Pl. While many cells would be needed to model the entire domain at a 10cm resolution, the more refined cells can be kept to the specific area of interest, and resolution in adjacent areas can be increased to coarser resolutions. As with the mesh sensitivity study, care is taken to ensure that adjacent mesh blocks differ in cell size by no more than a 2:1 ratio. This constraint helps reduce numerical errors and maintain stability and accuracy in the transfer of solution variables across mesh interfaces.

A total of 48 computational meshes were needed to model the full computational domain with a 10 cm cell resolution between houses. To speed up computation time, the governing equations within the meshes in the numerical simulation were computed in parallel using MPI. MPI is a standardized and portable protocol used for inter-process communication in parallel computing environments. Within FDS, MPI enables distributed-memory parallelization by assigning each of several meshes within a computational domain to its own dedicated process. During runtime, each MPI process independently solves governing equations over its assigned mesh while exchanging information at mesh boundaries with neighboring processes. This

exchange includes the transfer of scalar and vector field data required to maintain continuity and consistency across the global domain.

The use of MPI in FDS is critical for efficiently simulating large-scale or high-resolution fire scenarios, such as those encountered in WUI fire spread studies, where the computational demands can be substantial due to complex geometry, fine spatial resolution, and long simulation durations. Effective parallelization with MPI not only reduces wall-clock time but also enables the use of larger domains and finer grids that would be computationally prohibitive on a single processor. However, achieving optimal parallel performance depends on minimizing load imbalance and communication overhead, which necessitates careful mesh decomposition and MPI process allocation.

Meshes used to construct the computational domain each contained 27,648 cells. In total there were 46 MPI processes assigned to all meshes in the computational domain. 24 meshes had a 10 cm grid resolution, 13 meshes had a 20 cm grid resolution, 8 meshes had a 40 cm grid resolution, and three meshes had an 80 cm grid resolution. The 80 cm meshes had a reduced cell count as compared to the rest of the meshes in the domain and so are computed in serial with each other within a single MPI process.

Due to concerns in regards to numerical stability of the full-scale model with a 10 cm cell resolution, a second computational domain was created which has a finest cell resolution of 20 cm. Models using this domain are able to calculate results significantly quicker than the 10 cm resolution models, albeit without using the best resolution determined by the mesh sensitivity study described in Section 4.9.2. This configuration uses a total of 22 meshes, each computed in parallel with each other with MPI. 8 meshes have a 20 cm cell resolution, 7 meshes have a 40 cm cell resolution, and 7 meshes have an 80 cm cell resolution. Meshes in this domain each contain 7,680

cells. Although the model with this mesh distribution is not optimal, the difference compared to the optimal mesh (10 cm model) is not significant, less than 10%, as discussed above.

Chapter 5 Results and Discussion

As discussed in Chapter 4, multiple configurations of the full-scale fire model of 1267 and 1259 Nahale Pl were created and executed for comparison of results. Two sets of models were created for analysis of different burner configurations, whole wall and half wall to evaluate whether the FDS simulation is able to capture the ignition of the 1259 Nahale Pl building (Section 5.1). Additional simulation was conducted with trees removed from the computational domain to evaluate their contribution to fire spread between homes. Moreover, the sensitivities of ignition time to the exterior wall thermal and surface properties are investigated in Section 5.3.

5.1 Results from the Full-scale Models with Different Burner Configurations

The 10 cm model experienced numerous numerical convergence issues; therefore, the discussion will primarily focus on the simulation results from the 20 cm models. Although the 20 cm model is not optimal, the difference compared to the optimal mesh is not significant, less than 10%, as discussed above. The 20 cm model configurations were constructed on a grid consisting of 22 meshes, each with 7,680 cells. Simulations required approximately 44 hours to complete, with each mesh computed as a parallel MPI process, with three processors allocated per mesh. The 20 cm resolution window burner configuration encountered numerical instability issues. It could only be completed for approximately 1200 seconds of simulation after start, while the interior burner configuration resulted in a very low measured heat flux on the exterior wall of the target building. The following discussion of simulation results primarily focuses on the 20 cm models with full-wall and half-wall configurations. The simulation results for the window burner and interior burner configurations will be discussed at the end of this section.

Heat flux and surface temperature measurements are collected at the exterior wall of 1259 Nahale Pl on a 31 x 15 grid, measuring 5.8 m in the horizontal direction and 2.6 m in the vertical direction. Measuring devices have a separation distance of 0.2 m, equal to the local grid resolution. For post-simulation data processing, a spatial average “cell value” was computed over each grid cell by averaging the values collected at its four corner points. The average and maximum spatial averages of heat flux and wall surface temperature measured at the exterior wall of 1259 Nahale Pl are shown in Figures 5.1 and 5.2. At each time step, the average curve represents the mean of all cell averages across the target exterior wall of 1259 Nahale Pl, while the maximum curve represents the highest cell average among all cells at that time step.

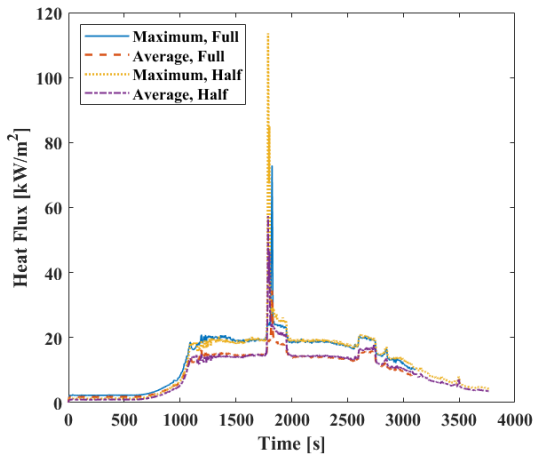


Figure 5.1 Heat Flux

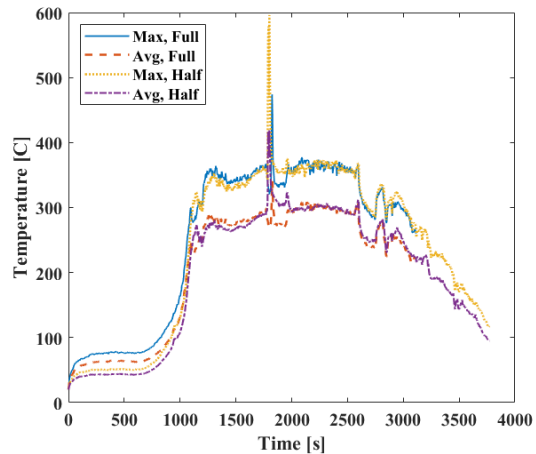


Figure 5.2 Wall Surface Temperature

For both configurations, the heat flux and temperature measured at the exterior wall begins to increase rapidly 750 seconds after the ignition of the house. At approximately 1100 seconds after ignition, maximum heat fluxes plateau at 20 kWm^{-2} , with average heat fluxes leveling off just slightly below 15 kWm^{-2} . At this same time, average and maximum wall temperatures have reached approximately $340 \text{ }^\circ\text{C}$ and $275 \text{ }^\circ\text{C}$, respectively. Roughly 30 minutes after 1267 Nahale Pl ignites, the heat flux reaches its maximum value. The full wall burner configuration produces a maximum heat flux of 72.9 kWm^{-2} , and the average heat flux across the wall goes as high as 34.5

kWm^{-2} . Maximum and average wall temperature produced by the full wall burner configuration at this time is $474\text{ }^{\circ}\text{C}$ and $340\text{ }^{\circ}\text{C}$. The half wall burner configuration produces a maximum heat flux of 113.6 kWm^{-2} , and the average heat flux across the wall goes as high as 57.4 kWm^{-2} . Maximum and average wall temperature produced by the half wall burner configuration at this time is $596\text{ }^{\circ}\text{C}$ and $420\text{ }^{\circ}\text{C}$. These peak values are reached not after a period of steady, sustained increase in heat flux and wall temperature, but rather as part of a sudden, sharp spike in these measurements. These peaks correspond to the observed ignition times for trees vegetative fuel between houses in the model.

An ignition temperature of $350\text{ }^{\circ}\text{C}$ is considered for this analysis, determined via experimentally obtained values for piloted ignition temperature of plywood [56]. While piloted ignition temperature is used for this analysis, the flames coming from 1267 Nahale Pl is at too great a separation distance to itself act as a pilot. However, smaller combustibles between the spaces such as flaming debris and smaller vegetative fuels are likely to have ignited during the fire and acted as pilots for this target surface, justifying the use of piloted ignition temperature as an ignition criterion. Ignition time is determined as the initial time at which the temperature in any given cell exceeds this threshold for at least 8 consecutive time steps (32 seconds). The half-wall burner configuration suggests an ignition time of 1720 s after the house ignites. The full-wall burner configuration suggests an ignition time of 1268 s after the house ignites. In the video recording, once the fire in 1267 Nahale Pl is fully developed, the unclear camera footage makes it difficult to determine the exact time and location of ignition. The best estimate of the ignition time for the fire scene is in the range of 1637 s to 1893 s, as indicated in Figure 5.3a and b, with likely ignition locations circled.



a. Fire Scene at t=1637s

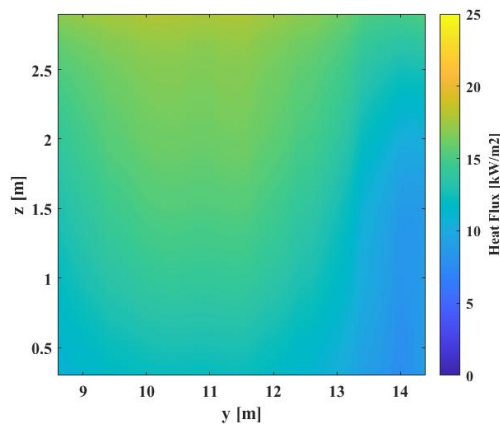


b. Fire Scene at t=1893s

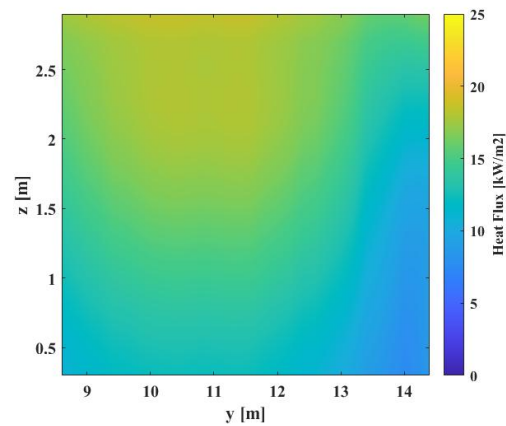
Figure 5.3 Corresponding Video Segment around the Estimated Ignition Time

For further clarity and contextualization of heat flux values presented in Figure 5.1 and temperature values presented in Figure 5.2, contour plots were created to visualize the distribution of heat flux and temperature across the exterior wall. Plots given for several select points throughout the simulation are shown in Figures 5.4 and

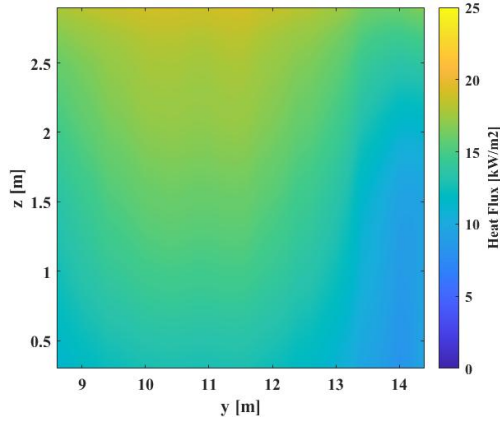
Figure 5.5 . The times selected correspond to the steady state of the house fire, with all design fires just reaching their maximum HRR, as well as the ignition times estimated for each configuration.



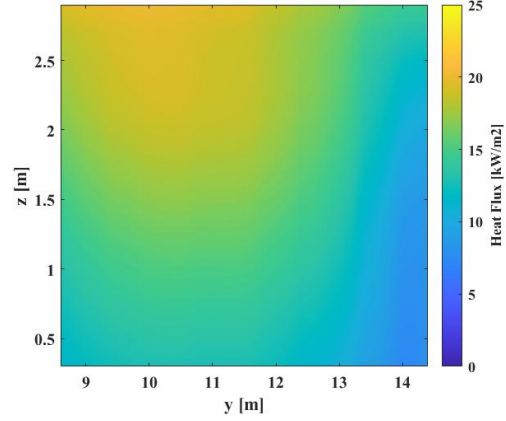
a. Heat Flux at Steady State Fire, Half Wall Burner Configuration (t=1496 s)



b. Heat Flux at Steady State Fire, Full Wall Burner Configuration (t=1496 s)

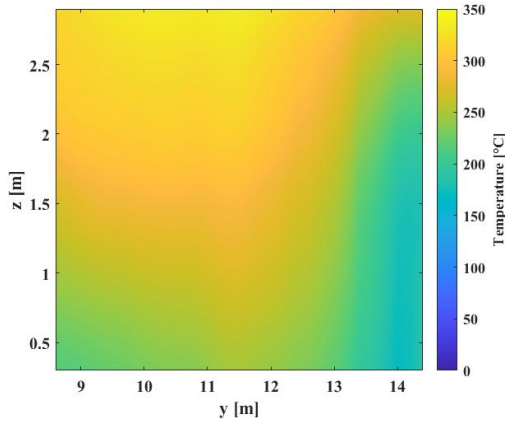


c. Heat Flux at Ignition, Half-Wall Burner Configuration (t=1720 s)

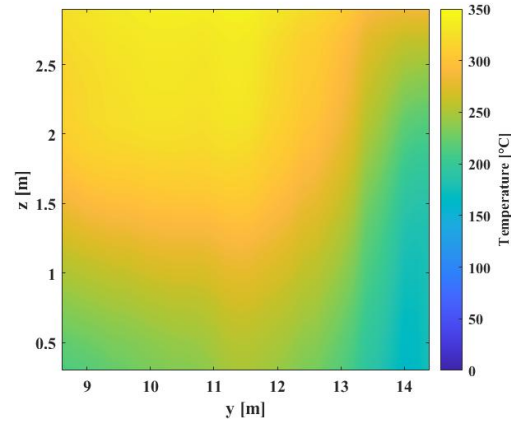


d. Heat Flux at Ignition, Full Wall Burner Configuration (t=1268 s)

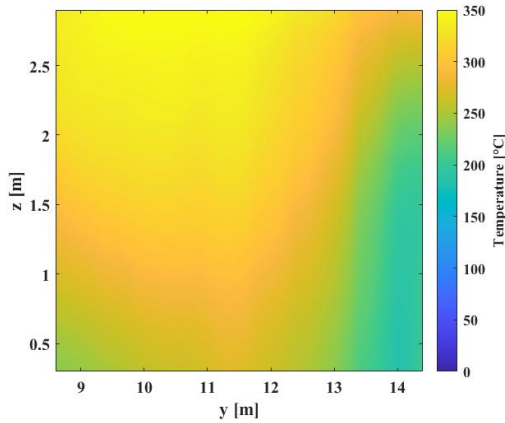
Figure 5.4 Heat Flux Contours, 20cm Cell Resolution



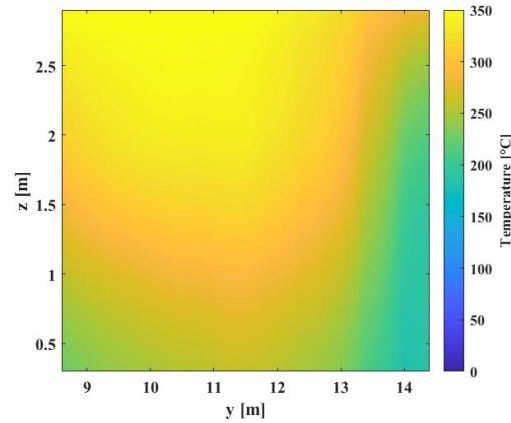
a. Temperature at Steady State Fire, Half-Wall Burner Configuration (t=1496s)



b. Temperature at Steady State Fire, Full-Wall Burner Configuration (t=1496s)



c. Wall Temperature at Ignition, Half Wall Burner Configuration (t=1720 seconds)



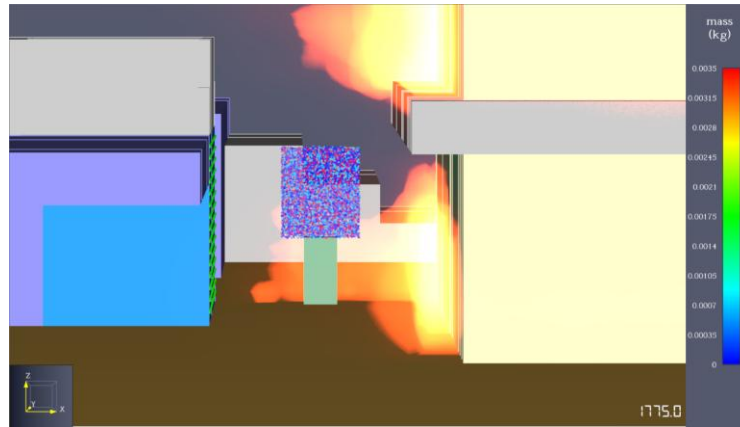
d. Wall Temperature at Ignition, Full Wall Burner Configuration (t=1268 seconds)

Figure 5.5 Wall Temperature Contours, 20cm Cell Resolution

In the video, all three trees ignited during the fire, but only one is visible in the camera footage, igniting at 2,070 s, seen in Figure 5.6. In the simulation, for example, with the half-wall burner configuration, the ignition of one of the trees between the houses is shown in Figure 5.7b. Note that only one of the three trees ignites during the simulation, which is inconsistent with observations from the fire scene and indicates that the model requires further improvement. The mass of the particles making up the tree can be seen decreasing rapidly as the tree ignites. All particles seen in Figure 5.7c have reached zero kg in mass, denoted by their dark blue color on the particle mass scale given on the right color bar of the figure. At 1,774 seconds in the FDS model, the wind shifted direction, blowing from 1267 Nahale Pl toward the tree and 1259 Nahale Pl; this occurred after the ignition of 1267 Nahale Pl in the FDS simulation (1,720 seconds in the simulation with the half-wall burner configuration). The onset of the wind-direction change at 1774 seconds, and the period during which the wind blew from 1267 Nahale Pl toward the tree, are closely linked to the subsequent ignition of vegetative fuels at 1781 seconds. This tree ignition in the FDS model coincides with the sharp increase in measured heat flux at the exterior wall of 1259 Nahale Pl (Figure 5.1).



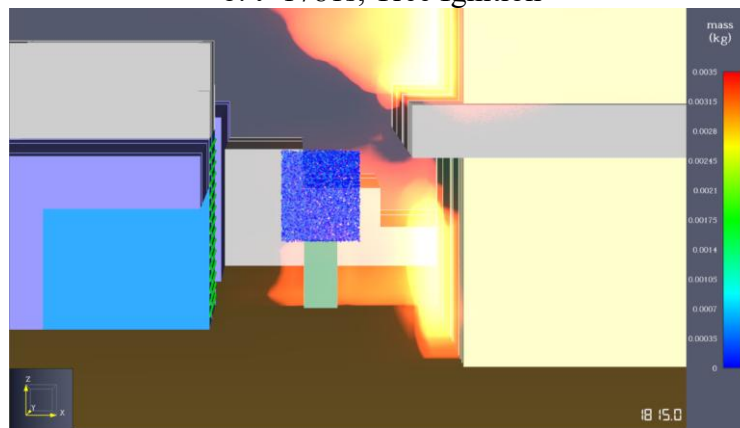
Figure 5.6 Tree Ignition (t=2070s)



a. $t = 1775$ s, Before Tree Ignition



b. $t=1781$ s, Tree Ignition

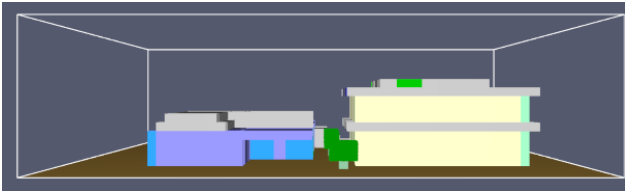


c. $t=1815$ s, After Tree Ignition

Figure 5.7 Tree Ignition, Half-Wall Burner

Shown in Figure 5.8 is a comparison of key times in the progression of the fire in the observed camera footage with the corresponding times in the FDS simulation. Times given correspond to the simulation start, full house fire growth, estimated ignition time of 1259 Nahale

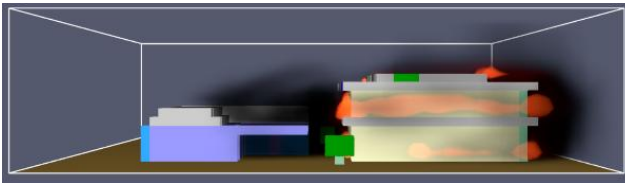
PI for the full-wall and half-wall burner configurations, and flaming ignition of vegetation. All simulation screenshots provided are sourced from the half-wall burner configuration, except for the time corresponding to estimated ignition from the full-wall burner configuration, which is sourced from its appropriate simulation.



a. Model Start, Simulation (t=0s)



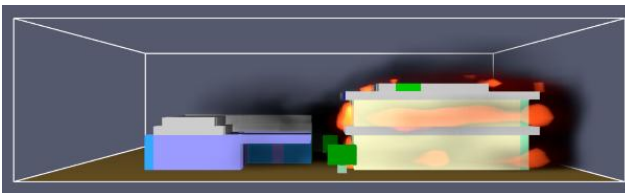
b. Fire Scene at t=0s



c. Full Fire Growth, Simulation (t=1141s)



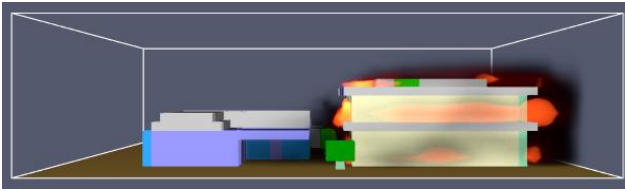
d. Fire Scene at t=1141s



e. Exterior Wall Ignition, Full Wall Configuration, Simulation (t=1268s)



f. Fire Scene at t=1268s



g. Exterior Wall Ignition, Half Wall Configuration, Simulation (t=1720s)



h. Fire Scene at t=1720s



i. Wind Direction Change and Vegetation Ignition, Simulation (t=1781s)



j. Fire Scene at t=1781s



k. Wind Change and Vegetation Ignition, Simulation, Smoke Excluded (t=1781s)

Figure 5.8 Video and FDS Model Comparison

The full-wall and half-wall burner configurations are considered as the most optimal configurations for the analysis of results. Examining video results produces an estimated ignition time of the exterior wall of 1259 Nahale Pl as being between 1637 and 1893 seconds after ignition of 1267 Nahale Pl. Analyzing the results of FDS simulations yields ignition times of 1268 and 1720 seconds for the full-wall and half-wall burner configurations, respectively. Both configurations produce ignition of vegetative fuels at 1781 seconds. Due to its stronger adherence to the observed estimated ignition time in the physical fire, the half-wall burner configuration is to be used in further analysis of results.

In the previous discussion, we did not cover the window burner configuration and the interior configuration. The window burner configuration encountered numerical instability errors at the 20 cm cell resolution. The specific cause of this instability could not be determined; however, the size of the windows along the walls of 1267 Nahale Pl was rather small when compared to the cell size, with some windows spanning over only a couple of cells, which led to issues with the computation of improperly or insufficiently resolved flame sources. Heat flux measurements for this configuration, compared with the full-wall and half-wall configurations at the 20 cm resolution up to the point of instability, are given in Figure 5.9. While heat flux values differ between the three configurations in the earlier stages of the simulation, both maximum and average spatial averages across all configurations tend to approach similar values.

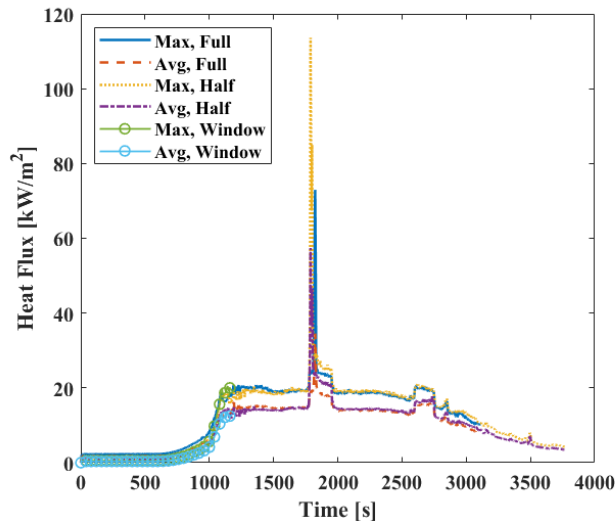


Figure 5.9 Window Heat Flux

For the interior configuration wherein burners were placed on the interior floors of 1267 Nahale Pl. Windows were placed at appropriate locations on the exterior walls according to the building configuration. Heat flux measurements from this configuration, as compared to the half-wall burner configuration, are shown in Figure 5.10. As evident by comparing the heat flux

measurements for the interior burner configuration with those from the half-wall burner configuration, the use of the interior burner configuration produced inaccurate results, significantly lower than exterior fires. In particular, FDS calculates very little heat radiated outwards from the compartment without explicitly-defined jet plumes at openings in the compartment. In compartment fires, the relative concentrations of gaseous fuel and oxygen may progress to the point where the environment is fuel-rich, where there is not enough oxygen present in the compartment to combust all fuel. At this point, gaseous fuel will leave the compartment, where they will entrain exterior oxygen and form a buoyant plume. Flames in FDS which ultimately reach the compartment openings do not automatically entrain oxygen from the domain surrounding the compartment and form a buoyant flame outside as they would in reality. Another reason is that the burning of the structures at a later stage involved the full enclosure of the building, which made the fire very intense and generated a large amount of heat that directly exposed the nearby structure. The interior burner configuration is unable to reproduce this behavior. Due to these deficiencies in modeling capabilities, the interior burner configuration is not considered for further analysis.

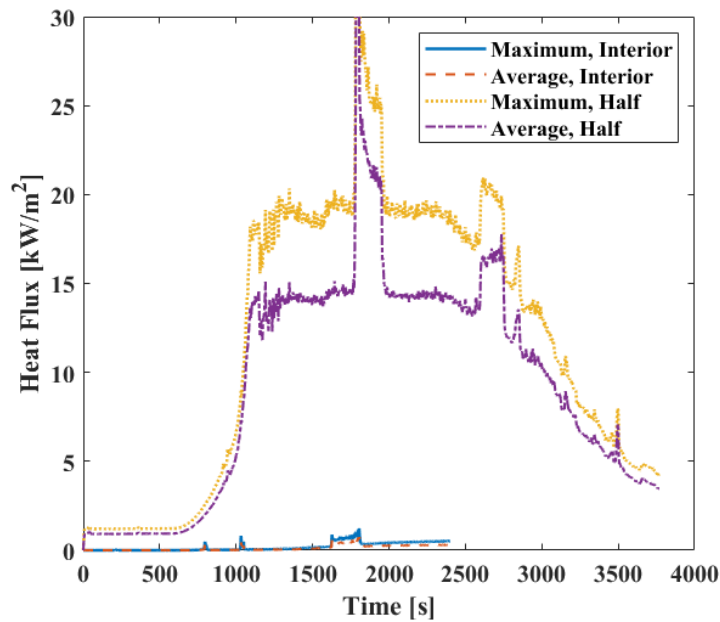


Figure 5.10 Interior Burner Configuration Heat Flux

5.2 Impact of Vegetation on Fire Spread between Structures

To further examine the impact of vegetative fuels on flame spread and heat transfer between houses, a separate model was created that excludes these fuels from the computational domain. This simulation was created using half-wall burners. The heat flux and temperature values measured on the exterior wall of the 1259 Nahale P1 in each simulation (half-wall burner configuration with and without trees) are compared in Figure 5.11.

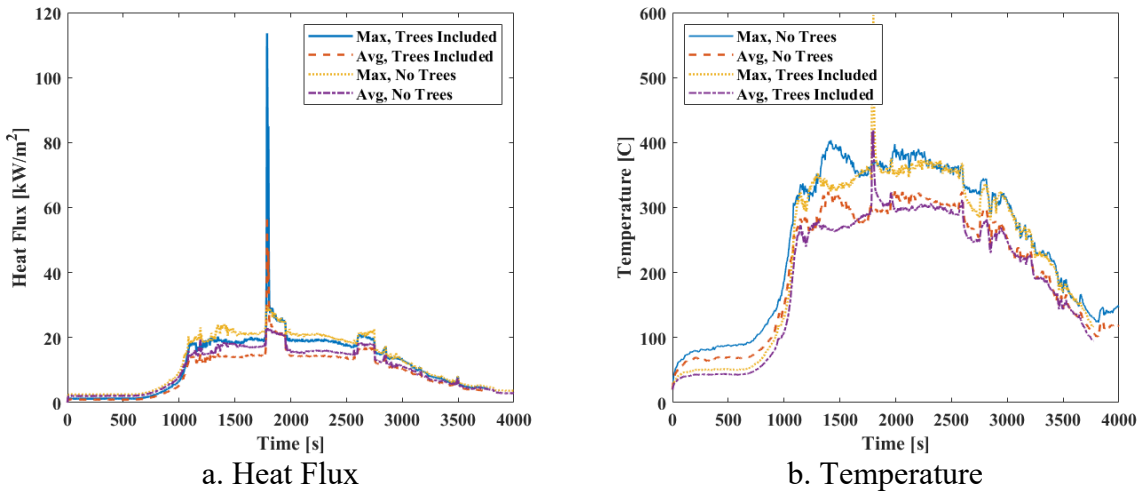


Figure 5.11 Measured Heat Flux, Trees Excluded

In the model without vegetative fuels, the peak heat flux measured along the exterior wall reach a peak maximum value of 29.5 kWm^{-2} , and the average value across the entire wall reaches a maximum of 23.0 kWm^{-2} . This represents a drastic decrease in heat flux as compared to the model configurations which include vegetative fuels. The drastic increase in heat flux at 1800 s is no longer present without the trees in the model, as there is no longer the secondary combustible fuel source to transmit heat to 1259 Nahale Pl in addition to what the combustion of 1267 Nahale Pl supplies. The peak maximum values of heat flux and wall temperature in models without trees (29.5 kW m^{-2} and 404°C , respectively) occur still at roughly the same time due to the impact of wind effects, particularly in that a change in wind direction associated with increased heat transfer from 1267 to 1259 Nahale Pl occurs at this time. Further discussion of wind effects is given in Section 5.3. It is worth noting that the removal of the trees between houses caused the steady heat fluxes measured at the exterior wall to be greater than those observed in the other simulations. This is due to the shielding that the trees provide target houses such as 1259 Nahale Pl from flaming sources such as 1267 Nahale Pl, as the heat that would typically be transferred to the tree is now transferred to the exterior wall.

5.3 Impact of Wind Direction on Fire Spread Between Structures

Examination of Figures 5.1 and 5.11 additionally reveals the impact of wind on the heat transfer between structures, particularly the wind direction. Figure 5.12 shows the half-wall heat flux measurements, with darker shading depicting the times when wind blew from 1267 Nahale Pl towards 1259 Nahale Pl.

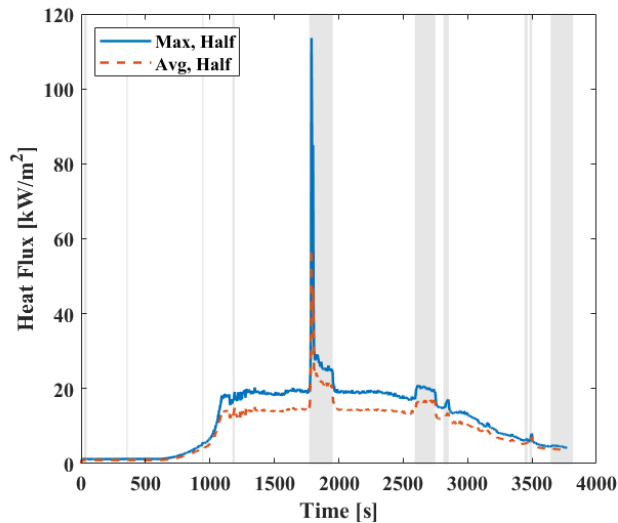


Figure 5.12 Heat Fluxes, Wind Overlay

These times are directly associated with significant increases in heat flux measured at the target exterior wall. It bears mentioning that the ignition of vegetative fuels (at 1781 seconds in the FDS simulation) between structures occurred at the onset of a wind direction shift at 1774 seconds after ignition of 1267 Nahale Pl. The coupling of the wind direction change with the ignition of vegetative fuels is sensible when considering fire dynamics. The vegetative fuels are represented with thermally thin particles, which cannot be easily heated and ignited with radiative heat transfer alone due to thermal losses to surrounding gases. As the wind changes direction and blows the fire towards the vegetation, there is a greater influence of convective heat transfer in the area, allowing for ignition of the thin particles.

5.4 Material Property Sensitivity Analysis

Ignition of the exterior wall of 1259 Nahale Pl is determined by the surface temperature of its outermost plywood layer. This surface temperature is sensitive to the assigned specific heat, thermal conductivity, density, and emissivity of plywood. The sensitivity study of temperature development to material properties allows for the determination of a probable range of ignition times for 1259 Nahale Pl.

A small-scale model was created in FDS for the sensitivity studies. The model, shown in Figure 5.13, introduces the half-wall burner average heat flux given in Figure 5.1 as a boundary condition to the yellow surface. The average heat flux was chosen over the maximum because it provides a more accurate representation when applied across the entire wall, whereas using the maximum value across the full wall geometry leads to unrealistically high temperature predictions. Wall dimensions, materials and layer thickness are identical to those used in the full-scale model. Wall surface temperature is measured and analyzed with the same process described in section 5.1 of this report.

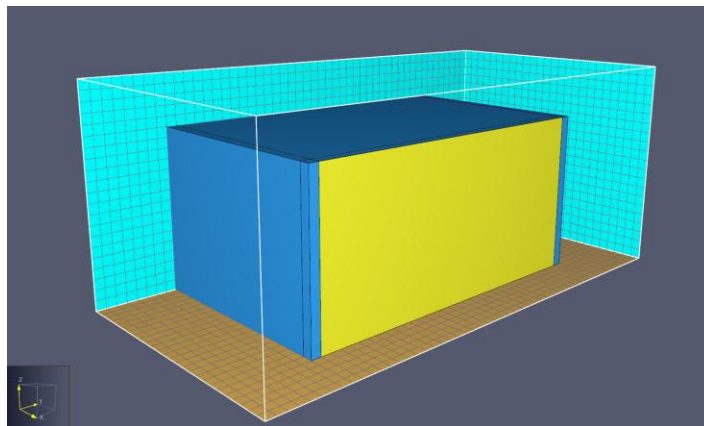


Figure 5.13 Property Sensitivity Model

Review of existing databases and literature yielded a range of accepted values for the specific heat, thermal conductivity, density, and emissivity of plywood. The ranges of the properties are given in Table 5.1.

Property	Minimum Value	Maximum Value
Specific Heat, c [kJkg ⁻¹ K ⁻¹]	1.261	1.607
Thermal Conductivity, k [Wm ⁻¹ K ⁻¹]	0.107	0.126
Density, ρ [kgm ⁻³]	500	600
Emissivity, ε	0.82	0.95

First, the plywood material used in the FDS wall construction is assigned either the minimum or maximum accepted value for each given parameter. This yields 16 different configurations for the sensitivity analysis. Sensitivity analysis results are shown in Figure 5.14.

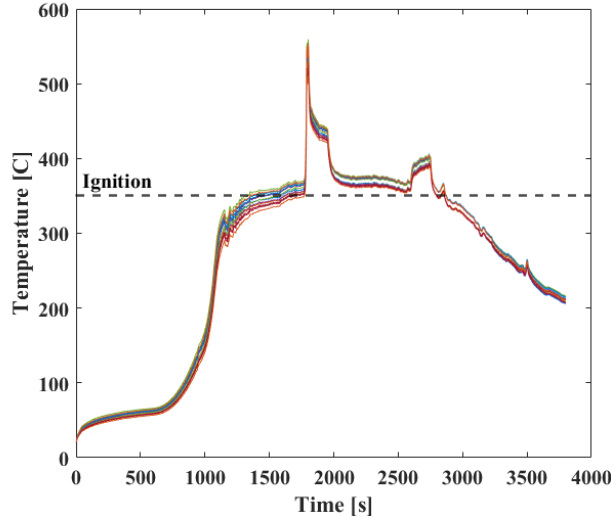


Figure 5.14 Sensitivity Analysis Temperature Development

Unlike the full-scale fire model, heat flux is applied to the wall in a spatially uniform fashion, and so discernment is not made between average and maximum wall temperature. It is important to note that the temperature profile may not accurately represent post-ignition

conditions, as the simulation does not account for the heat generated by pyrolysis and combustion of the exterior wall, which is not modeled. The temperature profiles given in Figure 5.13 establish a range of expected ignition times for 1259 Nahale Pl. Ignition times for each configuration are given in Table 5.2. The average predicted time to ignition was 1535 seconds, with a minimum and maximum predicted ignition time of 1330 and 1771 seconds, respectively. Ignition times in Table 5.2 show that the model results are most sensitive to changes in emissivity relative to property ranges given in Table 5.1.

Table 5.2 Predicted Ignition Times

Minimized Parameter(s)	Maximized Parameter(s)	Ignition Time [s]
c, k, ρ, ε	—	1592
k, ρ, ε	c	1626
k, ρ	c, ε	1353
ρ, ε	c, k	1687
ρ	c, k, ε	1471
ε	c, k, ρ	1771
—	c, k, ρ, ε	1585
k, ε	c, ρ	1687
k	c, ρ, ε	1471
c, k, ρ	ε	1330
c, ρ, ε	k	1611
c, ρ	k, ε	1349
c, ε	k, ρ	1645
c	k, ρ, ε	1418
c, k, ε	ρ	1611
c, k	ρ, ε	1349

For further analyzing the sensitivity of the ignition time to material properties, plywood material properties used in the base model as given in Table 4.2 were each increased and decreased by 10%. Temperature profiles are shown in Figure 5.15. Resulting times to ignition were compared with the estimated ignition time of the 20 cm resolution, half-wall burner configuration. The estimated ignition time for the base model in this case is 1611 s, which is the ignition time estimated by the simplified model with no property changes from the full model. Examining model

results shows that the ignition time is most sensitive to changes in the emissivity of the plywood, while the model is still relatively sensitive to changes in thermal conductivity. Ignition time has similar, non-sensitive behavior for changes to the specific heat and density of plywood. Among all configurations in this sensitivity study, the average time to ignition is 1625 seconds, while the minimum and maximum times to ignition are 1417 and 1778 seconds, respectively.

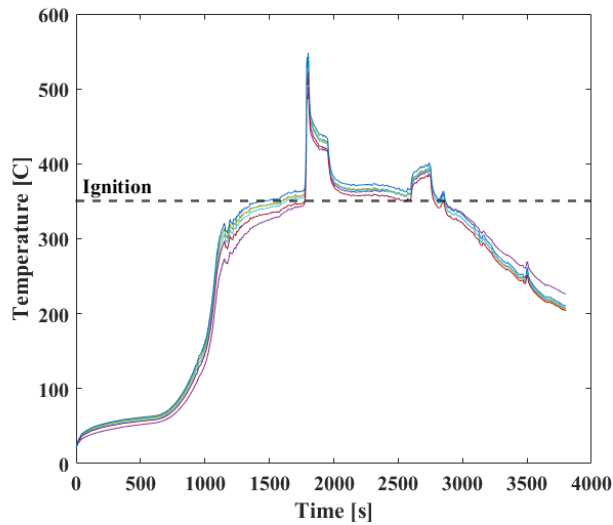


Figure 5.15 Sensitivity Analysis of Temperature Development

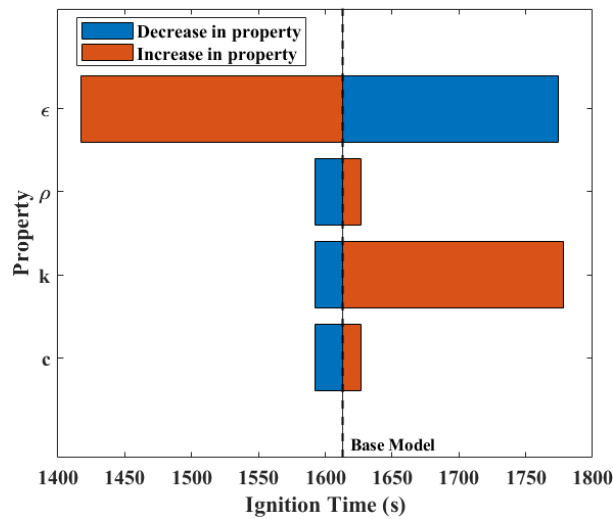


Figure 5.16 Material Property Adjustment Comparison

Chapter 6 Conclusion and Future Work

6.1 *Summary of Work*

This project aimed to replicate the burning of an individual residential structure in Lahaina. The goal was to validate the use of FDS for simulating structural ignition caused by the burning of an adjacent structure, using well-defined structural and vegetation fire sources. The model examines multiple configurations of burner distribution for structural fuel sources to determine optimal practice in future modeling efforts.

Four different configurations were investigated, including the full-wall burner configuration, half-wall burner configuration, window-burner configuration, and interior-burner configuration. An optically thin radiation model was used in those simulations. The full-wall and half-wall burner configurations are considered the most suitable. In terms of ignition-time accuracy, the half-wall model yields predictions (1720 seconds) closest to the video-based estimate (1637 seconds ~ 1893 seconds). Use of the interior burner configuration, rather than burners placed directly on the exterior of a building, was deemed not viable for complete structure fire modeling, resulting in very low incident heat flux on the exterior wall surface of the target building. Use of flames within the interior of a building, either through the use of a burner with a prescribed heat release rate or through individual modeling of fuel packages, may be more accurate in modeling compartment fires, which develop as flame spreads through a structure. As the fire develops further and beyond the compartment, in particular when the fire involves the burning of structure enclosure, the use of exterior burners as seen in this report (i.e., full-wall configuration and half-wall configuration) will be more accurate in modeling structural fires which consider fire dynamics around the exterior of a structure and increased heat transfer to neighboring structures and

combustibles. Configurations using smaller burners to represent heat transfer through windows exhibited instabilities. Before the point of non-convergence, the simulation results are similar to those from the wall configurations. Nevertheless, their potential should be further investigated for applications in modeling structure burning in WUI areas, as such fires ultimately involve the combustion of the entire structure, including the wood-frame enclosure.

The inclusion of vegetative fuels was deemed to be critical for accurate heat transfer calculations in WUI environments, as they significantly reduce separation distances between adjacent combustibles and provide additional, high-volume heat sources. Heat flux to surrounding structures was shown to significantly increase in the direction of wind flow, emphasizing the importance of a well-defined model for wind velocity and direction across a WUI environment for fire risk assessment purposes.

The sensitivity of ignition time to the properties of the exterior materials was also investigated. The results indicate that ignition time is highly sensitive to a material's surface emissivity, while temperature development is also significantly affected by variations in thermal conductivity. Variations in density and specific heat had a smaller impact on ignition time, but these properties should still be selected carefully to avoid inaccuracies.

6.2 *Limitations and Future Work*

Many difficulties and limitations were encountered with FDS, which offers suggestions for future work. Instabilities were encountered when examining many model configurations. Models configured at a 10-cm resolution encountered numerical instabilities at the time of full fire growth, which should be further investigated so that results may be examined at a resolution shown to be optimal by mesh convergence studies.

For the burner distribution configuration, although the half-wall burner arrangement can estimate the ignition time reasonably well, the overall flame size during structural burning remains smaller than observed in the tests. Future work should explore additional burner distribution configurations to better capture both the ignition time and the flame's shape and size.

The present work is limited by the use of the optically thin radiation model in FDS, which neglects reabsorption of radiation by gases and soots and may not accurately represent conditions in WUI fires with higher soot loading or optical thickness. While this choice increased the predicted heat flux and reduced the simulated ignition time to match observations better, its physical validity requires further investigation. If the optically thick mode is selected, additional sensitivity studies are needed for other radiative model parameters, such as background gas composition and path length.

Another limitation lies in the computational domain of the simulation. In this study, the domain was defined within a relatively constrained spatial extent, which may restrict the accurate representation of boundary effects, flow development, and heat transfer beyond the modeled region. Such limitations could influence the fidelity of predicted fire dynamics and structural response. Therefore, additional studies with larger or varied computational domains are necessary to systematically assess the sensitivity of the results to domain size and to ensure that the conclusions drawn are not artifacts of these constraints.

Of the three plumeria trees between 1267 and 1259 Nahale Pl, only one tree was ignited within the FDS model, despite all three having ignited during the Lahaina fire. Further work should be performed to ensure the accuracy of vegetative fuel implementation into FDS and ensure that all relevant fuel packages may ignite.

Due to scope and time constraints, the presence of windows on the exterior wall of 1259 Nahale Pl was not modeled within FDS. These windows would be a major contributor to heat transfer into the interior of the house, both before and after breakage. Breakage of windows along residential structures in WUI areas could allow for flame spread into and the ignition of the interior of the building. While the ignition of the exterior wall of 1259 Nahale Pl is observed in available footage, the timing of exterior window breakage and associated consequences cannot be confidently estimated and so are excluded from this model. Future work should review existing window breakage models or develop new ones, along with their implementation in FDS.

Bibliography

1. (2023) New Maui brush fire forces brief evacuation of Lahaina neighborhood. In: CBS News. <https://www.cbsnews.com/news/maui-brush-fire-evacuation-lahaina-neighborhood/>. Accessed 22 Sep 2023
2. Institute for Business I, Safety H (2023) IBHS Insights: Lahaina Fire – 2023
3. Maranghides A, Nazare S, Link E, et al (2023) NIST Outdoor Structure Separation Experiments (NOSSE) with wind
4. Maranghides A, Nazare S, Hedayati F, et al (2022) Structure Separation Experiments: Shed Burns without Wind
5. Maranghides A, Johnsson EL (2008) Residential structure separation fire experiments. Gaithersburg, MD
6. Himoto K, Shinohara M, Sekizawa A, et al (2018) A field experiment on fire spread within a group of model houses. *Fire Saf J* 96:105–114. <https://doi.org/10.1016/j.firesaf.2018.01.003>
7. Johnsson EL (2025) Wind-Driven Fire Spread to a Structure from Landscape Timbers
8. Ghaderi M, Ghodrati M, Sharples JJ (2021) Les simulation of wind-driven wildfire interaction with idealized structures in the wildland-urban interface. *Atmosphere (Basel)* 12:1–17. <https://doi.org/10.3390/atmos12010021>
9. Ganteaume A, Guillaume B, Girardin B, Guerra F (2023) CFD modelling of WUI fire behaviour in historical fire cases according to different fuel management scenarios. *Int J Wildland Fire* 32:363–379. <https://doi.org/10.1071/wf22162>
10. McGrattan K, McDermott R, Vanella M, et al (2025) Fire Dynamics Simulator Technical Reference Guide Volume 3: Validation. Gaithersburg, MD
11. McGrattan KB, McDermott R, Vanella M, et al (2024) Fire Dynamics Simulator Technical Reference Guide Volume 3. Gaithersburg, MD
12. Evans DD, Rehm RG, Baker ES Physics-Based Modeling for WUI Fire Spread-Simplified Model Algorithm for Ignition of Structures by Burning Vegetation
13. Shah R (2020) Ember Accumulation During Wildfires. *Young Scientists Journal*
14. Wickramasinghe A Physics-based simulation of firebrand and heat flux on structures in the context of AS3959
15. De Beer JA (2023) Experimental Analysis and Numerical Modeling of Ignition of Lignocellulosic Building Materials Subjected to Glowing Firebrand Piles
16. Cuzzillo BR, Pagni PJ (1998) Thermal breakage of double-pane glazing by fire. *Journal of Fire Protection Engineering* 9:1–11. <https://doi.org/10.1177/104239159800900101>
17. Keski-Rahkonen O (1988) Breaking of window glass close to fire. *Fire Mater* 12:61–69. <https://doi.org/https://doi.org/10.1002/fam.810120204>
18. Skelly M, Roby R, Beyler C (1991) An Experimental Investigation of Glass Breakage in Compartment Fires. *Journal of Fire Protection Engineering - J FIRE PROT ENG* 3:25–34. <https://doi.org/10.1177/104239159100300103>
19. Shields TJ, Silcock GWH, Flood MF (2001) Performance of a single glazing assembly exposed to enclosure corner fires of increasing severity. *Fire Mater* 25:123–152. <https://doi.org/https://doi.org/10.1002/fam.764>
20. Dembele S, Rosario R, Wen J, et al (2008) Simulation of Glazing Behavior in Fires using Computational Fluids Dynamics and Spectral Radiation Modeling. *Fire Safety Science* 9:1029–1039. <https://doi.org/10.3801/IAFSS.FSS.9-1029>

21. Dembélé S, Rosario RAF, Wen JX, et al (2007) Study of Glazing Behaviour in Fire Conditions Using Advanced Radiation Heat Transfer Model and Computational Fluid Dynamics. *Fire Safety Science* 7:93
22. Chu T, Jiang L, Usmani A (2023) Introducing an active opening strategy to mitigate large open-plan compartment fire development. *Fire Saf J* 141:103981. <https://doi.org/10.1016/j.firesaf.2023.103981>
23. Kerber S, Alkonis D (2025) Lahaina Fire Forward-Looking Report. <https://doi.org/10.60752/102376.28074944>
24. Sangal A, Powell TB, Meyer M, et al (2023) August 11, 2023 Maui wildfire news. In: CNN. <https://www.cnn.com/us/live-news/hawaii-maui-wildfires-08-11-23/index.html>. Accessed 6 Aug 2025
25. Piper I, Lee J, Izadi E, Sacks B (2023) Maui’s neglected grasslands caused Lahaina fire to grow with deadly speed. *Washington Post*
26. (2025) Invasive Grasses in Hawaii and Their Impact. In: Hawaii Invasive Species Council
27. Kim SE (2023) How Swaths of Invasive Grass Made Maui’s Fires So Devastating. *Smithsonian Magazine*
28. Simon M (2023) The Scary Science of Maui’s Wildfires. In: *Wired*
29. Rush C, Borenstein S, McDermott J (2023) Maui’s fire became deadly fast. Climate change, flash drought, invasive grass and more fueled it. In: *Associated Press*
30. Partyka G, Erdman B (2023) Meteorological Analysis of the August 2023 Maui Wildfires. In: *Global Modeling and Assimilation Office*
31. Yuan X, Wang Y, Ji P, et al A global transition to flash droughts under climate change
32. Juliano TW, Szasdi-Bardales F, Lareau NP, et al (2024) Brief communication: The Lahaina Fire disaster – how models can be used to understand and predict wildfires. *Natural Hazards and Earth System Sciences* 24:47–52. <https://doi.org/10.5194/nhess-24-47-2024>
33. Rush C, McAvoy A, Weber C (2023) Hawaii churches offer prayers for the dead and the missing after devastating Maui wildfires. In: *U.S. News*. <https://apnews.com/article/maui-hawaii-lahaina-deadliest-wildfire-fb2ebf6cd39c149a582b82eed6ac3930>. Accessed 6 Aug 2025
34. NOAA National Centers for Environmental Information (NCEI) (2025) U.S. Billion-Dollar Weather and Climate Disasters
35. Knodell K (2024) Cost of Lahaina, HI, Wildfires Reaches \$12 Billion. In: *FIREHOUSE*. <https://www.firehouse.com/operations-training/wildland/news/55132266/cost-of-lahaina-hi-wildfires-reaches-12-billion>. Accessed 6 Aug 2025
36. Chappell B (2023) “Miracle house” owner hopes it will serve as a base for rebuilding Lahaina. In: *NPR*
37. *Associated Press* (2024) Report finds ‘no evidence’ Hawaii officials prepared for Maui wildfire that killed 102 despite warnings. In: *CNN*
38. Dolan J, Nakano C, Hamilton M (2023) Maui death toll surpasses Paradise; deadliest U.S. wildfire in a century. In: *Los Angeles Times*
39. *UH News* (2025) UHERO: Maui wildfires trigger population loss, economic impact. In: *University of Hawai’i News*
40. McGrattan KB, McDermott R, Vanella M, et al (2024) *Fire Dynamics Simulator Technical Reference Guide Volume 1*. Gaithersburg, MD

41. McGrattan K, Hostikka S, Floyd J, et al (2024) Fire Dynamics Simulator (Sixth Edition). Gaithersburg, MD
42. AhPuck C (2000) 1259 Nahale St
43. (2019) 1267 Nahale Pl. In: Redfin. <https://www.redfin.com/HI/Lahaina/1267-Nahale-Pl-96761/home/88607949>. Accessed 19 Mar 2025
44. (2021) r603.9 Structural Sheathing. International Resident Code
45. (2014) International building code 2012
46. Plywood. In: UL Fire Safety Research Institute
47. (2021) Table 6 Thermal Conductivity, Specific Heat Capacity and Density. In: Integrated Energy Solutions. https://help.iesve.com/ve2021/table_6_thermal_conductivity__specific_heat_capacity_and_density.htm. Accessed 3 Aug 2025
48. Luche J, Mathis E, Rogaume T, et al (2012) High-density polyethylene thermal degradation and gaseous compound evolution in a cone calorimeter. *Fire Saf J* 54:24–35. <https://doi.org/10.1016/J.FIRESAF.2012.08.002>
49. Gong J, Zhu H, Zhou H, Stoliarov SI (2021) Development of a pyrolysis model for oriented strand board. Part I: Kinetics and thermodynamics of the thermal decomposition. *J Fire Sci* 39:190–204. <https://doi.org/10.1177/0734904120982887>
50. Gong J, Zhou H, Zhu H, et al (2021) Development of a pyrolysis model for oriented strand board: Part II—Thermal transport parameterization and bench-scale validation. *J Fire Sci* 39:477–494. <https://doi.org/10.1177/07349041211036651>
51. Hurley MJ (2016) SFPE handbook of fire protection engineering, Fifth edition. Springer, New York
52. Asphalt Shingles. In: UL Fire Safety Research Institute
53. AW (2015) Asio Residence
54. Babrauskas V, Grayson SJ (1992) Heat release in fires. Taylor & Francis, London, England
55. Weinschenk CG, Overholt KJ, Madrzykowski D (2014) Simulation of an Attic Fire in a Wood Frame Residential Structure - Chicago, IL. Gaithersburg, MD
56. Babrauskas V (2002) Ignition of Wood: A Review of the State of the Art. *Journal of Fire Protection Engineering - J FIRE PROT ENG* 12:163–189. <https://doi.org/10.1177/10423910260620482>